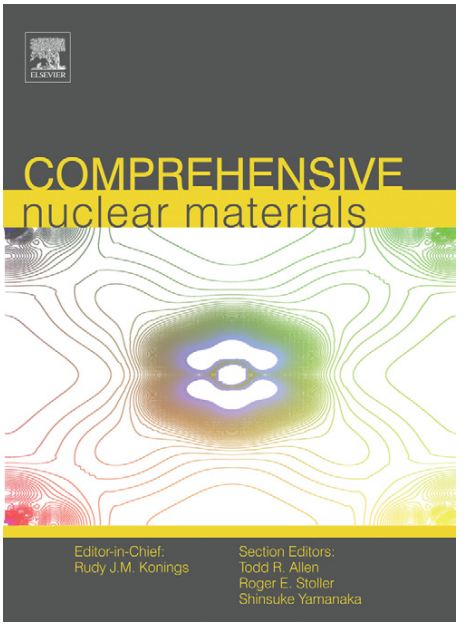

Nastar M. and Soisson F. (2012) Radiation-Induced Segregation. In: Konings R.J.M., (ed.) Comprehensive Nuclear Materials, volume 1, pp. 471-496 Amsterdam: Elsevier.

1.18 Radiation-Induced Segregation

M. Nastar and F. Soisson
Commissariat à l'Energie Atomique, DEN Service de Recherches de Métallurgie Physique, Gif-sur-Yvette, France

1.18.1	**Introduction**	472
1.18.2	**Experimental Observations**	473
1.18.2.1	Anthony's Experiments	473
1.18.2.2	First Observations of RIS	474
1.18.2.3	General Trends	475
1.18.2.3.1	Segregating elements	475
1.18.2.3.2	Segregation profiles: Effect of the sink structure	475
1.18.2.3.3	Temperature effects	476
1.18.2.3.4	Effects of radiation particles, dose, and dose rates	476
1.18.2.3.5	Impurity effects	476
1.18.2.4	RIS and Precipitation	476
1.18.2.5	RIS in Austenitic and Ferritic Steels	477
1.18.3	**Diffusion Equations: Nonequilibrium Thermodynamics**	479
1.18.3.1	Atomic Fluxes and Driving Forces	480
1.18.3.2	Experimental Evaluation of the Driving Forces	480
1.18.3.2.1	Local chemical potential	480
1.18.3.2.2	Thermodynamic databases	481
1.18.3.3	Experimental Evaluation of the Kinetic Coefficients	481
1.18.3.3.1	Interdiffusion experiments	482
1.18.3.3.2	Anthony's experiment	482
1.18.3.3.3	Diffusion during irradiation	482
1.18.3.3.4	Available diffusion data	483
1.18.3.4	Determination of the Fluxes from Atomic Models	483
1.18.3.4.1	Jump frequencies	483
1.18.3.4.2	Calculation of the phenomenological coefficients	484
1.18.4	**Continuous Models of RIS**	486
1.18.4.1	Diffusion Models for Irradiation: Beyond the TIP	486
1.18.4.1.1	Manning approximation	487
1.18.4.1.2	Interstitials	487
1.18.4.1.3	Analytical solutions at steady state	487
1.18.4.1.4	Concentration-dependent diffusion coefficients	488
1.18.4.2	Comparison with Experiment	488
1.18.4.2.1	Dilute alloy models	488
1.18.4.2.2	Austenitic steels	489
1.18.4.3	Challenges of the RIS Continuous Models	490
1.18.5	**Multiscale Modeling: From Atomic Jumps to RIS**	490
1.18.5.1	Creation and Elimination of Point Defects	490
1.18.5.2	Mean-Field Simulations	491
1.18.5.3	Monte Carlo Simulations	491
1.18.6	**Conclusion**	494
References		495

Comprehensive Nuclear Materials (2012), vol. 1, pp. 471-496

Abbreviations

AKMC	Atomic kinetic Monte Carlo
bcc	Body-centered cubic
DFT	Density functional theory
dpa	Displacement per atom
fcc	Face-centered cubic
IASCC	Irradiation-assisted stress corrosion cracking
IK	Inverse Kirkendall
MIK	Modified inverse Kirkendall
nn	Nearest neighbor
NRT	Norgett, Robinson, and Torrens
PPM	Path probability method
RIP	Radiation-induced precipitation
RIS	Radiation-induced segregation
SCMF	Self-consistent mean field
TEM	Transmission electron microscopy
TIP	Thermodynamics of irreversible processes

Symbols

D	Diffusion coefficient
L_{ij}, L or L-coefficient	Phenomenological coefficient

1.18.1 Introduction

Irradiation creates excess point defects in materials (vacancies and self-interstitial atoms), which can be eliminated by mutual recombination, clustering, or annihilation of preexisting defects in the microstructure, such as surfaces, grain boundaries, or dislocations. As a result, permanent irradiation sustains fluxes of point defects toward these point defect sinks and, in case of any preferential transport of one of the alloy components, leads to a local chemical redistribution. These radiation-induced segregation (RIS) phenomena are very common in alloys under irradiation and have important technological implications. Specifically in the case of austenitic steels, because Cr depletion at the grain boundary is suspected to be responsible for irradiation-assisted stress corrosion, a large number of experiments have been conducted on the RIS dependence on alloy composition, impurity additions, irradiation flux and time, irradiation particles (electrons, ions, or neutrons), annealing treatment before irradiation, and nature of grain boundaries.[1–5]

The first RIS models generally consisted of application of Fick's laws to reproduce two specific effects of irradiation: diffusion enhancement due to the increase of point defect concentration, and the driving forces associated with point defect concentration gradients. According to these models, RIS is controlled by kinetic coefficients D or L (defined below) relating atomic fluxes to gradients of concentration or chemical potentials. It was shown that these coefficients are best defined in the framework of the thermodynamics of irreversible processes (TIPs) within the linear response theory. RIS models were then separated into two categories: models restricted to dilute alloys, and models developed for concentrated alloys.

From the beginning until now, the dilute alloy models have benefited from progress made in the diffusion theory.[6] The explicit relations between the phenomenological coefficients L and the atomic jump frequencies have been established, at least for alloys with first nearest neighbor (nn) interactions. In principle, such relations allow the immediate use of *ab initio* atomic jump frequencies and lead to predictive RIS models.[7]

While the progress of RIS models of dilute alloys is closely related to that of diffusion theory, most segregation models for concentrated alloys still use oversimplified diffusion models based on Manning's relations.[8] This is mainly because the jump sequences of the atoms are particularly complex in a multicomponent alloy on account of the multiple jump frequencies and correlation effects that are involved. Only very recently has an interstitial diffusion model been developed that could account for short-range order effects, including binding energies with point defects.[9,10] Emphasis has so far been placed on comparisons with experimental observations. The continuous RIS models have been modified to include the effect of vacancy trapping by a large-sized impurity or the nature and displacement of a specific grain boundary. Most of the diffusivity coefficients of Fick's laws are adjusted on the basis of tracer diffusion data. Paradoxically, the first RIS models were more rigorous[11] than the present ones in which thermodynamic activities, particularly some of the cross-terms, are oversimplified. In this review, we go back to the first models starting from the linear response theory, albeit slightly modified, to be able to reproduce the main characteristics of an irradiated alloy. It is then possible to rely on the diffusion theories developed for concentrated alloys.

Then again, lattice rate kinetic techniques[12–14] and atomic kinetic Monte Carlo (AKMC) methods[15–17]

have become efficient tools to simulate RIS. Thanks to a better knowledge of jump frequencies due to the recent developments of *ab initio* calculations, these simulations provide a fine description of the thermodynamics as well as the kinetics of a specific alloy. Moreover, information at the atomic scale is precious when RIS profiles exhibit oscillating behavior and spread over a few tens of nanometers.

Discoveries and typical observations of RIS are illustrated in the first section. In the second section, the formalism of TIP is used to write the alloy flux couplings. It is explained that fluxes can be estimated only partially from diffusion experiments and thermodynamic data. An alternative approach is the calculation of fluxes from the atomic jump frequencies. The third section presents more specifically the continuous RIS models separated into the dilute and concentrated alloy approaches. The last section introduces the atomic-scale simulation techniques.

1.18.2 Experimental Observations

1.18.2.1 Anthony's Experiments

RIS was predicted by Anthony,[18] in 1969, a few years before the first experimental observations: a rare case in the field of radiation effects. The prediction stemmed from an analogy with nonequilibrium segregation observed in aluminum alloys quenched from high temperature. Between 1968 and 1970, in a pioneering work in binary aluminum alloys, Anthony and coworkers[18–22] systematically studied the nonequilibrium segregation of various solute elements on the pyramidal cavities formed in aluminum after quenching from high temperature. They explained this segregation by a coupling between the flux of excess vacancies toward the cavities and the flux of solute (Figure 1). Nonequilibrium segregation had been previously observed by Kuczynski *et al.*[23] during the sintering of copper-based particles and by Aust *et al.*[24] after the quenching of zone refined metals.

Anthony suggested that similar coupling should produce nonequilibrium segregation in alloys under irradiation.[18,19] He predicted that the segregation should be much stronger than after quenching because under irradiation, the excess vacancy concentration and the resulting flux can be sustained for very long times.[19,25] As for the cavities formed by vacancy condensation in alloys under irradiation, which result in the swelling phenomenon (**Chapter 1.03, Radiation-Induced Effects on Microstructure** and **Chapter 1.04, Effect of Radiation on Strength and Ductility of Metals and Alloys**), he pointed out that with solute and solvent atoms of different sizes, segregation should generate strains around the voids.[25] Finally, he predicted intergranular corrosion in austenitic steels and zirconium alloys, resulting from possible solute depletion near grain boundaries.[25]

Anthony also presented a detailed discussion on nonequilibrium segregation mechanisms, in the framework of the TIP,[18–21] showing that the nonequilibrium tendencies are controlled by the phenomenological coefficients L_{ij} of the Onsager matrix, which can be – in principle – computed from vacancy jump frequencies (see below **Section 1.18.3**). Clarifying previous discussions on nonequilibrium segregation mechanisms,[23,24] he considered two limiting cases for the coupling between solute and vacancy fluxes in an A–B alloy (at the time, he did not apparently consider the coupling between solute and interstitial fluxes and its possible contribution to RIS). In both cases, the total flux of atoms must be equal and in the direction opposite to the vacancy flux:

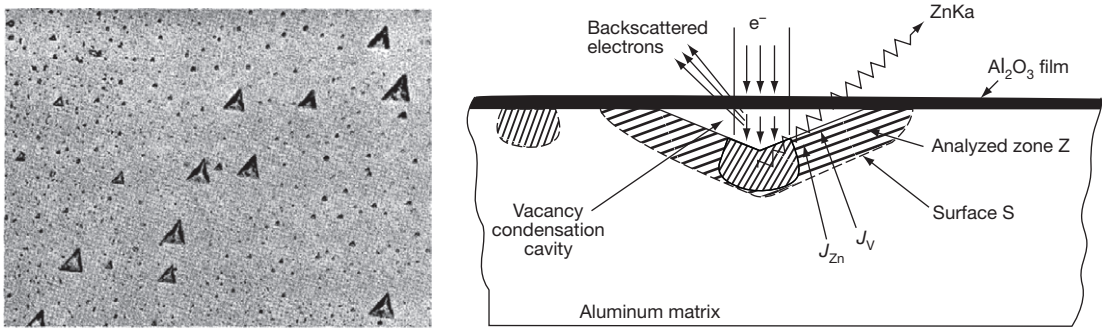

Figure 1 One of Anthony's experiments. After quenching of an Al–Zn alloy, vacancies condense in small pyramidal cavities (left), under an Al_2O_3 thin film covering the surface. Electronic probe measurements reveal enrichments in Zn around the cavities. Reproduced from Anthony, T. R. *J. Appl. Phys.* **1970**, *41*, 3969–3976.

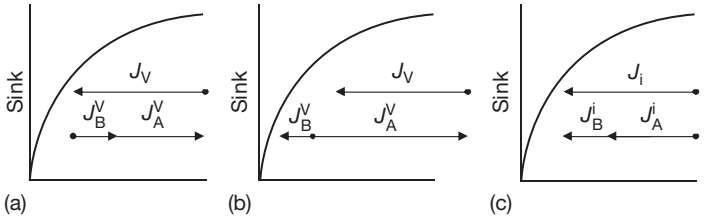

Figure 2 Radiation-induced segregation mechanisms due to coupling between point defect and solute fluxes in a binary A–B alloy. (a) An enrichment of B occurs if $d_{BV} < d_{AV}$ and a depletion if $d_{BV} > d_{AV}$. (b) When the vacancies drag the solute, an enrichment of B occurs. (c) An enrichment of B occurs when $d_{BI} > d_{AI}$.

1. If both A and B fluxes are in the direction opposite to the vacancy flux (**Figure 2(a)**), one can expect a depletion of B near the vacancy sinks if the vacancy diffusion coefficient of B is larger than that of A ($d_{BV} > d_{AV}$); in the opposite case ($d_{BV} < d_{AV}$), one can expect an enrichment of B (it is worth noting that this was essentially the explanation proposed by Kuczynski *et al.*[23] in 1960).
2. But A and B fluxes are not necessarily in the same direction. If the B solute atoms are strongly bound to the vacancies and if a vacancy can drag a B atom without dissociation, the vacancy and solute fluxes can be in the same direction (**Figure 2(b)**): this was the explanation proposed by Aust *et al.*[24] In such a case, an enrichment of B is expected, even if $d_{BV} > d_{AV}$.

1.18.2.2 First Observations of RIS

In 1972, Okamoto *et al.*[26] observed strain contrast around voids in an austenitic stainless steel Fe–18Cr–8Ni–1Si during irradiation in a high-voltage electron microscope. They attributed this contrast to the segregation strains predicted by Anthony. This is the first reported experimental evidence of RIS. Soon after, a chemical segregation was directly measured by Auger spectroscopy measurements at the surface of a similar alloy irradiated by Ni ions.[27]

It was then realized that if the solute concentration near the point defect sinks reaches the solubility limit, a local precipitation would take place. In 1975, Barbu and Ardell[28] observed such a radiation-induced precipitation (RIP) of an ordered Ni_3Si phase in an undersaturated Ni–Si alloy.

The analysis of strain contrast and concentration profiles measured by Auger spectroscopy suggested that undersized Ni and Si atoms (which can be more easily accommodated in interstitial sites) were diffusing toward point defect sinks, while oversized atoms (such as Cr) were diffusing away. Such a trend, later confirmed in other austenitic steels and nickel-based alloys,[29] led Okamoto and Wiedersich[27] to conclude that RIS in austenitic steels was due to the migration of interstitial–solute complexes, and they proposed this new RIS mechanism, in addition to the ones involving vacancies (**Figure 2(c)**). Then again, Marwick[30] explained the same experimental observations by a coupling between fluxes of vacancies and solute atoms, pointing out that thermal diffusion data showed Ni to be a slow diffuser and Cr to be a rapid diffuser in austenitic steels. We will see later that, in spite of many experimental and theoretical studies, the debate on the diffusion mechanisms responsible for RIS in austenitic steels is not over.

Following these debates on RIS mechanisms, it became common to refer to the situation illustrated in **Figure 2(a)** as segregation by an inverse Kirkendall (IK) effect (the term was coined by Marwick[30] in 1977) and to the one in **Figure 2(b)** as segregation by drag effects, or by migration of vacancy–solute complexes. In the classical Kirkendall effect,[31] a gradient of chemical species produces a flux of defects. It occurs typically in interdiffusion experiments in A–B diffusion couples, when A and B do not diffuse at the same speed. A vacancy flux must compensate for the difference between the flux of A and B atoms, and this leads to a shift of the initial A/B interface (the Kirkendall plane). The IK effect is due to the same diffusion mechanisms but corresponds to the situation where the gradient of point defects is imposed and generates a flux of solute. The distinction between RIS by IK effect and RIS by migration of defect–solute complexes, initially proposed for the vacancy mechanisms, was soon generalized to interstitial fluxes by Okamoto and Rehn.[32,33] RIS in dilute alloys, where solute–defect binding energies are clearly defined and often play a key role, is commonly explained by diffusion of solute–defect complexes, while the IK effect is often more useful to explain RIS in concentrated alloys. This distinction

is reflected in the modeling of RIS (see Section 1.18.3). However, it is clear that RIS can occur in dilute alloys without migration of solute–defect fluxes. Moreover, such a terminology and sharp distinction can be somewhat misleading; the mechanisms are not mutually exclusive. In the case of undersized B atoms, for example, a strong binding between interstitial and B atoms can lead to a rapid diffusion of B by the interstitial (IK effect with $D_{Bi} > D_{Ai}$) and to the migration of interstitial–solute complexes. More generally, one can always say that RIS results from an IK effect, in the sense that it occurs when a gradient of point defects produces a flux of solute. Nevertheless, because they are widely used, we will refer to these terms at times when they do not create confusion.

1.18.2.3 General Trends

Many experimental studies of RIS were carried out in the 1970s in model binary or ternary alloys, as well as in more complex and technological alloys (especially in stainless steels). It became apparent quite early on that RIS was a pervasive phenomenon, occurring in many alloys and with any kind of irradiating particle (ions, neutrons, or electrons). Extensive reviews can be found in Russell,[1] Holland *et al.*,[2] Nolfi,[3] Ardell,[4] and Was[5]: here, we present only the general conclusions that can be drawn from these studies.

1.18.2.3.1 Segregating elements

From the previous discussion, it is clear that it is difficult to predict the segregating element in a given alloy because of the competition between several mechanisms and the lack of precise diffusion data (especially concerning interstitial defects). As will be shown in Section 1.18.3, only the knowledge of the phenomenological coefficients L_{ij} provides a reliable prediction of RIS. Nevertheless, on the basis of the body of RIS experimental studies, several general rules have been proposed. In dilute binary AB alloys, thermal self-diffusion coefficients D^{A}_{A*} and impurity diffusion coefficients D^{A}_{B*} are generally well known, at least at high temperatures. Tracer diffusion or intrinsic diffusion coefficients in some concentrated alloys are also available.[34] RIS experiments do not reveal a systematic depletion of the fast-diffusing and enrichment of the slow-diffusing elements near the point defect sinks[4,29]: this suggests that the IK effect by vacancy diffusion is usually not the dominant mechanism. On the other hand, it seems that a clear correlation exists between RIS and the size effect[33]; undersized atoms usually segregate at point defect sinks, oversized atoms usually do not. This suggests that interstitial diffusion could control the RIS, at least for atoms with a significant size effect. There are some exceptions: in Ni–Ge and Al–Ge alloys, the segregation of oversized solute atoms has been observed. Nevertheless, as pointed out by Rehn and Okamoto,[33] no case of depletion of undersized solute atoms in dilute alloys has ever been reported. According to Ardell,[4] this holds true even today.

1.18.2.3.2 Segregation profiles: Effect of the sink structure

Segregation concentration profiles induced by irradiation display some specific features. They can spread over large distances – a few tens of nanometers (see examples in Russell[1] and Okamoto and Rehn[29]) – while equilibrium segregation is usually limited to a few angstroms. This is due to the fact that they result from a dynamic equilibrium between RIS fluxes and the back diffusion created by the concentration gradient at the sinks, while the scale of equilibrium segregation profiles is determined by the range of atomic interactions. Equilibrium profiles are usually monotonic, except for the oscillations, which can appear – with atomic wavelengths – in alloys with ordering tendencies.[35] Segregation profiles observed in transient regimes are often nonmonotonic because of the complex interaction between concentration gradients of point defects and solutes. A typical example is shown in Section 1.18.5.3, where an enrichment of solute is observed near a point defect sink, followed by a smaller solute depletion between the vicinity of sink and the bulk. In this particular case, the depletion is due to a local increase in vacancy concentration, which results from the lower interstitial concentration and recombination rate.

Other kinds of nonmonotonic profiles are sometimes observed, with typical 'W-shapes.' In some austenitic or ferritic steels, a local enrichment of Cr at grain boundaries survives during the Cr depletion induced by irradiation (see below). This could result from a competition between opposite equilibrium and RIS tendencies. However, the extent of the Cr enrichment often seems too wide to be simply due to an equilibrium property (around 5 nm, see, e.g., Sections 1.18.2.5 and 1.18.5.3).

RIS profiles at grain boundaries are sometimes asymmetrical, which has been related to the migration of boundaries resulting from the fluxes of point defects under irradiation.[37,38] The segregation is affected by the atomic structure and the nature of the sinks. It has been clearly shown that RIS in

austenitic steels is much smaller at low angles and special grain boundaries than at large misorientation angles,[39,40] the latter being much more efficient point defect sinks than the former.

1.18.2.3.3 Temperature effects

RIS can occur only when significant fluxes of defects towards sinks are sustained, which typically happens only at temperatures between 0.3 and 0.6 times the melting point. At lower temperatures, vacancies are immobile and point defects annihilate, mainly by mutual recombination. At higher temperatures, the equilibrium vacancy concentration is too high; back diffusion and a lower vacancy supersaturation completely suppress the segregation. Temperature can also modify the direction of the RIS by changing the relative weight of the competing mechanisms, which do not have the same activation energy. In Ni–Ti alloys, for example, the enrichment of Ti at the surface below 400 °C has been attributed to the migration of Ti–V complexes, and the depletion observed at higher temperatures should result from a vacancy IK effect.[41]

1.18.2.3.4 Effects of radiation particles, dose, and dose rates

RIS can be observed for very small irradiation doses; an enrichment of ~10% of Si has been measured, for example, at the surface of an Ni–1%Si alloy, after a dose of 0.05 dpa at 525 °C.[32] Such doses are much lower than those required for radiation swelling[5] or ballistic disordering effects.[42]

Increasing the radiation flux, or dose rate, directly results in higher point defect concentrations and fluxes towards sinks. The transition between RIS regimes is then shifted toward a higher temperature. But because point defect concentrations slowly evolve with the radiation flux (typically, proportional to its square root[43] in the temperature range where RIS occurs), a high increase is needed to get a significant temperature shift.

Radiation dose and dose rate are usually estimated in dpa and dpa s^{-1}, respectively, using the Norgett, Robinson, and Torrens model,[44] especially when a comparison between different irradiation conditions is desired. It is then worth noting that the amount of RIS observed for a given dpa is usually larger during irradiation by light particles (electrons or light ions) than by heavy ones (neutrons or heavy ions). In the latter case, point defects are created by displacement cascades in a highly localized area, and a large fraction of vacancies and interstitials recombine or form point defect clusters. The fraction of the initially produced point defects that migrate over long distances and could contribute to RIS is decreased. On the contrary, during irradiation by light particles, Frenkel pairs are created more or less homogeneously in the material, and a larger fraction survive to migrate (**Figure 3**).[45]

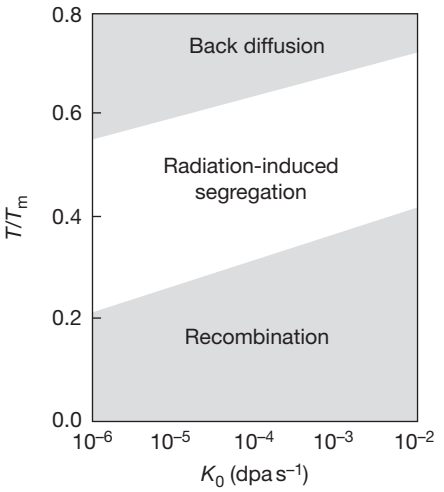

Figure 3 Temperature and dose rate effect on the radiation-induced segregation.

1.18.2.3.5 Impurity effects

The addition of impurities has been considered as a possible way to control the RIS in alloys, for example, in austenitic steels. The most common method is the addition of an oversized impurity, such as Hf and Zr, in stainless steels,[46] which should trap the vacancies (and, in some cases, the interstitials), thus increasing the recombination and decreasing the fluxes of defects towards the sinks.

1.18.2.4 RIS and Precipitation

As mentioned above, one of the most spectacular consequences of RIS is that it can completely modify the stability of precipitates and the precipitate microstructure.[47] When the local solute concentration in the vicinity of a point defect sink reaches the solubility limit, RIP can occur in an overall undersaturated alloy. RIP of the γ'-Ni_3Si phase is observed, for example, in Ni–Si alloys[28] at concentrations well below the solubility limit (Ni_3Si is an ordered $L1_2$ structure and can be easily observed in dark-field image in transmission electron microscopy (TEM)). In this case, it is believed that RIS is due to the preferential occupation of interstitials by undersized Si atoms.[28] The γ'-phase

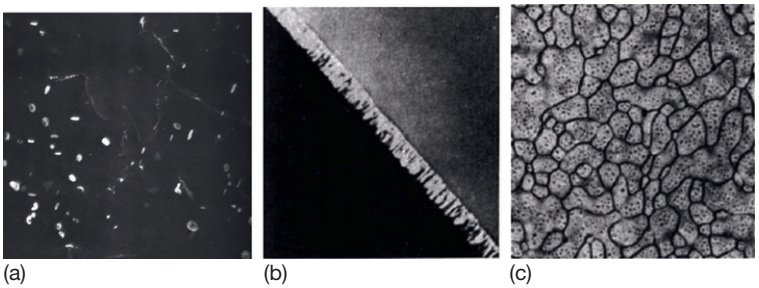

Figure 4 Formation of Ni_3Si precipitates in undersaturated solid solution under irradiation (a) in the bulk on preexisting dislocations and at interstitial dislocations (courtesy of A. Barbu), (b) at grain boundaries, and (c) at free surfaces. Reproduced from Holland, J. R.; Mansur, L. K.; Potter, D. I. *Phase Stability During Radiation*; TMS-AIME: Warrendale, PA, 1981.

can be observed on the preexisting dislocation network, at dislocation loops formed by self-interstitial clustering,[28] at free surfaces[45] or grain boundaries.[48] The fact that the γ'-phase dissolves when irradiation is stopped clearly reveals the nonequilibrium nature of the precipitation. This is also shown by the toroidal contrast of dislocation loops (**Figure 4(a)**): the γ'-phase is observed only at the border of the loop on the dislocation line where self-interstitials are annihilated; when the loop grows, the ordered phase dissolves at the center of the loop, which is a perfect crystalline region where no flux of Si sustains the segregation.

In supersaturated alloys, the irradiation can completely modify the precipitation microstructure. It can dissolve precipitates located in the vicinity of sinks when RIS produces a solute depletion. For example, in Ni–Al alloys,[49] dissolution of γ'-precipitates is observed around the growing dislocation loops due to the Al depletion induced by irradiation (**Figure 5**), and in supersaturated Ni–Si alloys, Si segregation towards the interstitial sinks produces dissolution of the homogeneous precipitate microstructure in the bulk, to the benefit of the precipitate layers on the surfaces[28] (**Figure 6**) and grain boundaries.[50]

In the previous examples, RIS was observed to produce a heterogeneous precipitation at point defect sinks. But homogeneous RIP of coherent precipitates has also been observed, for example, in Al–Zn alloys.[51] Cauvin and Martin[52] have proposed a mechanism that explains such a decomposition. A solid solution contains fluctuations of composition. In case of attractive vacancy–solute and interstitial–solute interactions, a solute-enriched fluctuation tends to trap both vacancies and interstitials, thereby favoring mutual recombination. The point defect concentrations then decrease, producing a flux of new defects toward the fluctuation. If the coupling with solute flux is positive, additional solute atoms arrive on the enriched fluctuations, and so it continues, till the solubility limit is reached.

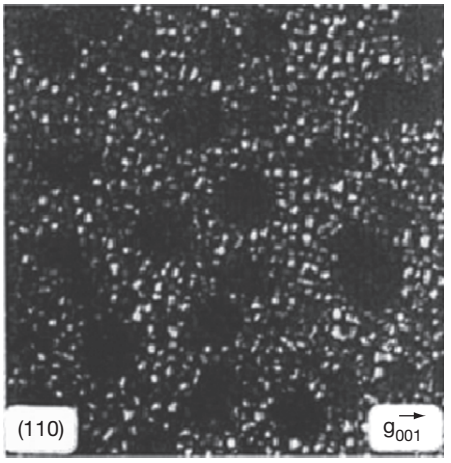

Figure 5 Dissolution of γ' near dislocation loop precipitates in Ni–Al under irradiation. Reproduced from Holland, J. R.; Mansur, L. K.; Potter, D. I. *Phase Stability During Radiation*; TMS-AIME: Warrendale, PA, 1981.

1.18.2.5 RIS in Austenitic and Ferritic Steels

We have seen that RIS was first observed in austenitic steels on the voids that are formed at large irradiation doses and lead to radiation swelling. The depletion of Cr at grain boundaries is suspected to play a role in irradiation-assisted stress corrosion cracking (IASCC); this is one of the many technological concerns related to RIS. The enrichment of Ni and the depletion of Cr can also stabilize the austenite near the sinks, and favor the austenite → ferrite transition in the matrix.[29] The segregation of minor elements can lead to the formation of γ'-precipitates (as in Ni–Si alloys), or various $M_{23}C_6$ carbides and other phases.[1,29]

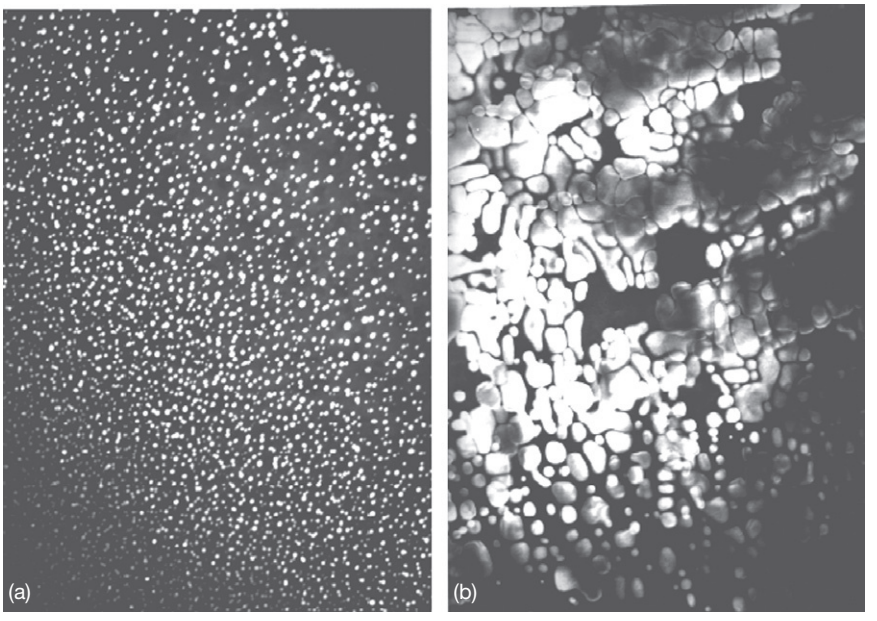

Figure 6 Precipitate microstructure in Ni–Si alloys: the homogeneous distribution observed during thermal aging (a) is dissolved under electron irradiation and the surfaces of the transmission electron microscopy sample are covered by Ni_3Si precipitates. (b) Ni–12%Si alloy under 1 MeV electron irradiation at 500 °C, after a dose of 5×10^{-5} dpa. Courtesy of A. Barbu.

The segregation of major elements always involves an enrichment of Ni and a depletion of Cr at sinks over a length scale that depends on the alloy composition and irradiation conditions.[5] The contribution of various RIS mechanisms is still debated. It is not clear whether it is the IK effect driven by vacancy fluxes, as suggested by the thermal diffusion coefficients $D_{Ni} < D_{Fe} < D_{Cr}$,[30] or the migration of interstitial–solute complexes, resulting in the segregation of undersized atoms,[29] that is dominant. Some models of RIS take into account only the first mechanism,[5] while others predict a significant contribution of interstitials.[12] For the segregation of minor elements, the size effect seems dominant, with an enrichment of undersized atoms (e.g., Si[27]) and a depletion of oversized atoms (e.g., Mo[53]) (**Figure 7**).

The effect of minor elements on the segregation behavior of major ones has been pointed out since the first experimental studies[29]; the effect of Si and Mo additions has been interpreted as a means of increasing the recombination rate by vacancy trapping. As previously mentioned, oversized impurity atoms, such as Hf and Zr, could decrease the RIS.[46]

RIS in ferritic steels has recently drawn much attention, because ferritic and ferrite martensitic steels are frequently considered as candidates for the future Generation IV and fusion reactors.[54]

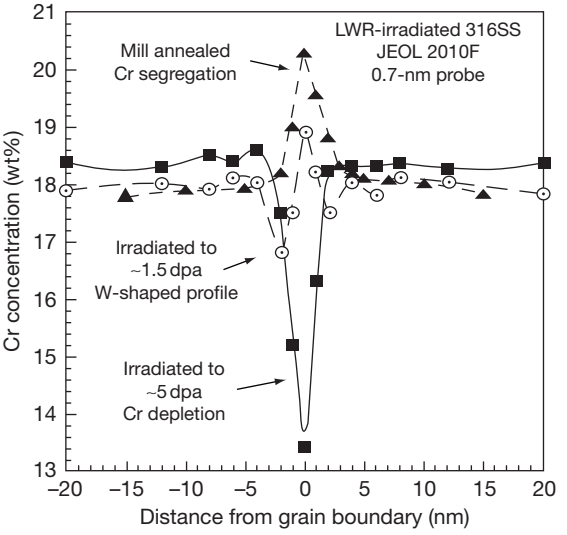

Figure 7 Thermal and radiation-induced segregation profiles in 316 stainless steel. Reproduced from Bruemmer, S. M.; Simonen, E. P.; Scott, P. M.; Andresen, P. L.; Was, G. S.; Nelson, J. L. *J. Nucl. Mater.* **1999**, *274*, 299–314.

Experimental studies are more difficult in these steels than in austenitic steels, especially because of the complex microstructure of these alloys. Identification of the general trends of RIS behavior in these alloys

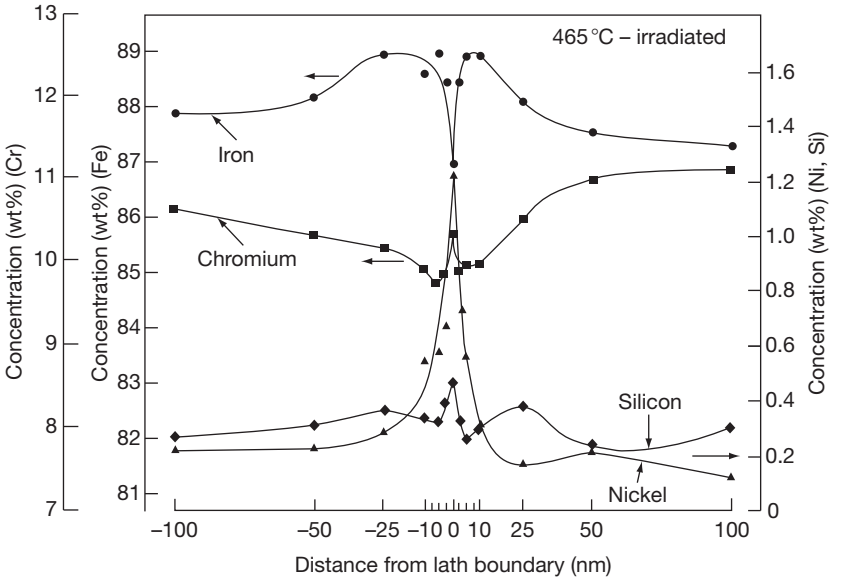

Figure 8 Concentration profiles of Cr, Ni, Si, and Fe on either side of a lath boundary in 12% Cr martensitic steel after neutron irradiation to 46 dpa at 465 °C. Reproduced from Little, E. *Mater. Sci. Technol.* **2006**, *22*, 491–518.

appears to be very difficult.[55] Nevertheless, in some highly concentrated alloys, a depletion of Cr and an enrichment of Ni have been observed, reminding us of the general trends in austenitic steels[54] (**Figure 8**). The RIS mechanisms are still poorly understood. The segregation of P at grain boundaries has been observed and, as in austenitic steels, the addition of Hf has been found to reduce the Cr segregation.[55]

1.18.3 Diffusion Equations: Nonequilibrium Thermodynamics

In pure metals, the evolution of the average concentrations of vacancies C_V and self-interstitials C_I are given by:

$$\frac{dC_V}{dt} = K_0 - RC_IC_V - \sum_s k_{Vs}^2 D_V (C_V - C_V^{eq})$$
$$\frac{dC_I}{dt} = K_0 - RC_IC_V - \sum_s k_{Is}^2 D_I C_I \qquad [1]$$

where K_0 is the point defect production rate (in dpa s^{-1}) proportional to the radiation flux, R is the recombination rate, and D_V and D_I are the point defect diffusion coefficients. The third terms of the right hand side in eqn [1] correspond to point defect annihilation at sinks of type s. The 'sink strengths' k_{Vs}^2 and k_{Is}^2 depend on the nature and the density of sinks and have been calculated for all common sinks, such as dislocations, cavities, free surfaces, grain boundaries, etc.[56,57] The evolution of point defect concentrations depending on the radiation fluxes and sink microstructure can be modeled by numerical integration of eqn [1], and steady-state solutions can be found analytically in simple cases.[43]

The evolution of concentration profiles of vacancies, interstitials, and chemical elements α in an alloy under irradiation are given by

$$\frac{\partial C_V}{\partial t} = -\mathrm{div}\, J_V + K_0 - RC_IC_V - \sum_s k_{Vs}^2 D_V [C_V - C_V^{eq}]$$
$$\frac{\partial C_I}{\partial t} = -\mathrm{div}\, J_I + K_0 - RC_IC_V - \sum_s k_{Is}^2 D_I C_I$$
$$\frac{\partial C_\alpha}{\partial t} = -\mathrm{div}\, J_\alpha \qquad [2]$$

The basic problem of RIS is the solution of these equations in the vicinity of point defect sinks, which requires the knowledge of how the fluxes J_α are related to the concentrations. Such macroscopic equations of atomic transport rely on the theory of TIP. In this chapter, we start with a general description of the TIP applied to transport. Atomic fluxes are written in terms of the phenomenological coefficients of diffusion (denoted hereafter by L_{ij} or, simply, L) and the driving forces. The second part is

devoted to the description of a few experimental procedures to estimate both the driving forces and the L-coefficients. In the last part, we present an atomic-scale method to calculate the fluxes from the knowledge of the atomic jump frequencies.

1.18.3.1 Atomic Fluxes and Driving Forces

Within the TIP,[58,59] a system is divided into grains, which are supposed to be small enough to be considered as homogeneous and large enough to be in local equilibrium. The number of particles in a grain varies if there is a transfer of particles to other grains. The transfer of particles α between two grains is described by a flux $\mathcal{J}_\alpha$, and the temporal variation of the local α concentration is given by the continuity equation

$$\frac{\partial C_\alpha}{\partial t} = -\mathrm{div}\,\mathcal{J}_\alpha \qquad [3]$$

The flux of species α between grains i and j is assumed to be a linear combination of the thermodynamic forces, $X_\beta = (\mu_\beta^j - \mu_\beta^i)/k_B T$ (i.e., of the gradient of chemical potentials $\nabla\mu_\beta$) where μ_β^i is the chemical potential of species β on site i, T the temperature, and k_B the Boltzmann constant. Variables X_β represent the deviation of the system from equilibrium, which tend to be decreased by the fluxes:

$$\mathcal{J}_\alpha = -\sum_\beta L_{\alpha\beta} X_\beta \qquad [4]$$

The equilibrium constants are the phenomenological coefficients, and the Onsager matrix $(L_{\alpha\beta})$ is symmetric and positive. When diffusion is controlled by the vacancy mechanism, atomic fluxes are, by construction, related to the point defect flux:

$$\mathcal{J}_V = -\sum_\alpha \mathcal{J}_\alpha^V \qquad [5]$$

As gradients of chemical potential are independent, eqn [5] leads to some relations between the phenomenological coefficients and, if we choose to eliminate the $L_{V\beta}^V$ coefficients, we obtain an expression for the atomic fluxes:

$$\mathcal{J}_\alpha^V = -\sum_\beta L_{\alpha\beta}^V (X_\beta - X_V) \qquad [6]$$

Under irradiation, diffusion is controlled by both vacancies and interstitials. The flux of interstitials is also deduced from the atomic fluxes:

$$\mathcal{J}_I = \sum_\beta \mathcal{J}_\beta^I \qquad [7]$$

Vacancy and interstitial contributions to the atomic fluxes are assumed to be additive:

$$\mathcal{J}_\alpha = -\sum_\beta L_{\alpha\beta}^V (X_\beta - X_V) - \sum_\beta L_{\alpha\beta}^I (X_\beta + X_I) \qquad [8]$$

While thermodynamic data is usually available for the determination of driving forces, it is very difficult to determine the whole set of the L-coefficients from diffusion data. In the first part of the chapter, we define the driving forces as a function of concentration gradients. Then, we present the experimental diffusion coefficients in terms of the L-coefficients and thermodynamic driving forces. The last part of the section shows how to use first-principle calculations for building atomic jump frequency models to calculate macroscopic fluxes of specific alloys.

1.18.3.2 Experimental Evaluation of the Driving Forces

1.18.3.2.1 Local chemical potential

The thermodynamic state equation defines a chemical potential of species i as the partial derivative of the Gibbs free energy G of the alloy, with respect to the number of atoms of species i, that is, N_i. The resulting chemical potential is a function of the temperature and molar fractions (also called concentrations) of the alloy components, $C_i = N_i/N$, N being the total number of atoms. TIP postulates that local chemical potentials depend on local concentrations via the thermodynamic state equation. A chemical potential gradient $\nabla\mu_i$ of species i is then equal to

$$\frac{\nabla\mu_i}{k_B T} = \frac{1}{k_B T}\sum_j \frac{1}{C_j}\left(C_j \frac{\partial\mu_i}{\partial C_j}\right)\nabla C_j \qquad [9]$$

where C_i is the local concentration of species i. In a binary alloy, concentration gradients of the two components are exactly opposite. The chemical potential gradient of component i is then proportional to the concentration gradient:

$$\frac{\nabla\mu_i}{k_B T} = \frac{\Phi_i}{C_i}\nabla C_i \qquad [10]$$

where Φ_i is called the thermodynamic factor. Furthermore, the Gibbs–Duhem relationship[58] leads to interdependent chemical potential gradients:

$$\sum_{k=1,r} C_k \nabla\mu_k = 0 \qquad [11]$$

where the sum runs over the number of species. Therefore, in a binary alloy there is one thermodynamic factor left:

$$\frac{\nabla\mu_i}{k_B T} = \frac{\Phi}{C_i}\nabla C_i \qquad [12]$$

where $\Phi = \Phi_A = \Phi_B$. Note, that an alloy at finite temperature contains point defects. They are currently assumed to be at equilibrium with the local alloy composition, with the local chemical potential equal to zero. When calculating the thermodynamic factor, point defect concentration gradients are neglected. During irradiation, although point defects are not at equilibrium, one assumes that eqn [12] continues to be valid.

Under irradiation, additional driving forces are involved. They correspond to the gradients of vacancy and interstitial chemical potentials, which are usually written in terms of their equilibrium concentrations C_V^{eq} and C_I^{eq} respectively:

$$\mu_V = k_B T \ln(C_V/C_V^{eq}) \text{ and } \mu_I = k_B T \ln(C_I/C_I^{eq}) \qquad [13]$$

leading to an expression of the associated driving force[11]:

$$\frac{\nabla\mu_V}{k_B T} = \frac{1}{C_V}\nabla C_V - \frac{\xi_{VA}}{C_A}\nabla C_A \text{ with } \xi_{VA} = \frac{\partial \ln C_V^{eq}}{\partial \ln C_A} \qquad [14]$$

The interstitial driving force has the same form, except that letter V is replaced by letter I. Note, that the equilibrium point defect concentrations may vary with the local alloy composition and stress. Although the variation of the equilibrium vacancy concentration is expected to be mainly chemical, the change of the elastic forces due to a solute redistribution at sinks should not be ignored for the interstitials.[11] Due to the lack of experimental data, Wolfer[11] introduced the equilibrium vacancy concentration as a contribution to a mean vacancy diffusion coefficient expressed in terms of the chemical tracer diffusion coefficients. Composition-dependent tracer diffusion coefficients could then account for the change of equilibrium vacancy concentration, with respect to the local composition.

Within the framework of the TIP, a thermodynamic factor depends on the local value but not on the spatial derivatives of the concentration field. The use of this formalism for continuous RIS models deserves discussion. Indeed, a typical RIS profile covers a few tens of nanometers so that the cell size used to define the local driving forces does not exceed a few lattice parameters. Such a mesoscale chemical potential is expected to depend not only on the local value, but also on the spatial derivatives of the concentration field. According to Cahn and Hilliard,[60] the free-energy model of a nonuniform system can be written as a volume integral of an energy density made up of a homogeneous term plus interface contributions proportional to the squares of concentration gradients. Thus, all continuous RIS models that are derived from TIP retain only the homogeneous contribution to the energy density and cannot reproduce interface effects and diffuse-interface microstructures. In particular, an equilibrium segregation profile near a surface is predicted to be flat.

1.18.3.2.2 Thermodynamic databases

The thermodynamic factor in eqn [12] is proportional to the second derivative of the Gibbs free energy G of the alloy, with respect to the molar fraction of one of the components. It can be calculated on the basis of thermodynamic data. A database such as CALPHAD[61] builds free-energy composition functions of the alloy phases from thermodynamic measurements (specific heats, activities, etc.). When available, the phase diagrams are used to refine and/or to assess the thermodynamic model. Although the CALPHAD free-energy functions are sophisticated functions of temperature and composition, it is interesting to study the simple case of a regular solution model. In the case of a binary alloy $A_{1-C}B_C$ with a clustering tendency, the Gibbs free energy is equal to

$$G = 2k_B T_c C(1-C) + k_B TC \ln(C) + k_B T(1-C)\ln(1-C) \qquad [15]$$

where T_c is the critical temperature and C is the alloy composition. The regular solution approximation leads to a concentration-dependent thermodynamic factor equal to

$$\Phi = 1 - 4C(1-C)\frac{T_c}{T} \qquad [16]$$

where concentration C now corresponds to a local concentration of B atoms, which varies in space and time.

1.18.3.3 Experimental Evaluation of the Kinetic Coefficients

The L-coefficients characterize the kinetic response of an alloy to a gradient of chemical potential. In practice, what is imposed is a composition gradient.

Chemical potential gradients, and therefore the fluxes, are assumed to be proportional to concentration gradients, (eqn [9]) leading to the generalized Fick's laws

$$\mathcal{J}_i = -\sum_j D_{ij} \nabla C_j \qquad [17]$$

A diffusion experiment consists of measurement of some of the terms of the diffusivity matrix D_{ij}. These terms cannot be determined one by one because at least two concentration gradients are involved in a diffusion experiment. Note, that the L-coefficients can be traced back only if the whole diffusivity matrix and the thermodynamic factors are known. Furthermore, most of the diffusion experiments are performed in thermal conditions and do not involve the interstitial diffusion mechanism.

In the following section, two examples of thermal diffusion experiments are introduced. Then, a few irradiation diffusion experiments are reviewed. The difficulty of measuring the whole diffusivity matrix is emphasized.

1.18.3.3.1 Interdiffusion experiments

In an interdiffusion experiment, a sample A (mostly composed of A atoms) is welded to a sample B (mostly composed of B atoms) and annealed at a temperature high enough to observe an evolution of the concentration profile. According to eqn [12], the flux of component i in the reference crystal lattice is proportional to its concentration gradient:

$$\mathcal{J}_i = -D_i \nabla C_i \qquad [18]$$

where the so-called intrinsic diffusion coefficient D_i is a function of the phenomenological coefficients and the thermodynamic factor:

$$D_i = \left(\frac{L_{ii}^{V}}{C_i} - \frac{L_{ij}^{V}}{C_j} \right) \Phi \qquad [19]$$

An interdiffusion experiment consists of measurement of the intrinsic diffusion coefficients as a function of local concentration. The resulting intrinsic diffusion coefficients are observed to be dependent on the local concentration. Within the TIP, while the driving forces are locally defined, the L-coefficients are considered as equilibrium constants. It is not easy to ensure that the experimental procedure satisfies these TIP hypotheses, especially when concentration gradients are large, and the system is far from equilibrium. When measuring diffusion coefficients, one implicitly assumes that a flux can be locally expanded to first order in chemical potential gradients around an averaged solid solution defined by the local concentration. Starting from atomic jump frequencies and applying a coarse-grained procedure, a local expansion of the flux has been proved to be correct in the particular case of a direct exchange diffusion mechanism.[62]

An interdiffusion experiment is not sufficient to characterize all the diffusion properties. For example, in a binary alloy with vacancies, in addition to the two intrinsic diffusion coefficients, another diffusion coefficient is necessary to determine the three independent coefficients L_{AA}, L_{AB}, and L_{BB}.

1.18.3.3.2 Anthony's experiment

Anthony set up a thermal diffusion experiment involving vacancies as a driving force[18–22,25,63] in aluminum alloys. The gradient of vacancy concentration was produced by a slow decrease of temperature. At the beginning of the experiment, the ratio between solute flux and vacancy flux is the following:

$$\frac{\mathcal{J}_B}{\mathcal{J}_V} = -\frac{L_{BB}^{V} + L_{AB}^{V}}{L_{AA}^{V} + L_{BB}^{V} + 2L_{AB}^{V}} \qquad [20]$$

The volume of the cavity and the amount of solute segregation nearby yield a value for the flux ratio. Note, that secondary fluxes induced by the formation of a segregation profile are neglected in the present analysis.

This experiment, combined with an interdiffusion annealing, could be a way to estimate the complete Onsager matrix. Unfortunately, the same experiment does not seem to be feasible in most alloys, especially in steels. In general, vacancies do not form cavities, and solute segregation induced by quenched vacancies is not visible when the vacancy elimination is not concentrated on cavities.

1.18.3.3.3 Diffusion during irradiation

In the 1970s, some diffusion experiments were performed under irradiation.[64] The main objective was to enhance diffusion by increasing point defect concentrations and thus facilitate diffusion experiments at lower temperatures. Another motive was to measure diffusion coefficients of the interstitials created by irradiation. In general, the point defects reach steady-state concentrations that can be several orders of magnitude higher than the thermal values. In pure metals, some experiments were reliable enough to provide diffusion coefficient values at temperatures that were not accessible in thermal conditions.[64]

The analysis of the same kind of experiments in alloys happened to be very difficult. A few attempts were made in dilute alloys that led to unrealistic values of solute–interstitial binding energies.[65] However, a direct simulation of those experiments using an RIS diffusion model could contribute to a better knowledge of the alloy diffusion properties.

Another technique is to use irradiation to implant point defects at very low temperatures. A slow annealing of the irradiated samples combined with electrical resistivity recovery measurement highlights several regimes of diffusion; at low temperature, interstitials with low migration energies diffuse alone, while at higher temperatures, vacancies and point defect clusters also diffuse. Temperatures at which a change of slope is observed yield effective migration energies of interstitials, vacancies, and point defect clusters.[66] *In situ* TEM observation of the growth kinetics of interstitial loops in a sample under electron irradiation is another method of determining the effective migration of interstitials.[67]

1.18.3.3.4 Available diffusion data

Interdiffusion experiments have been performed in austenitic and ferritic steels.[34] The determination of the intrinsic diffusion coefficients requires the measurement of the interdiffusion coefficient and of the Kirkendall speed for each composition.[68] In general, an interdiffusion experiment provides the Kirkendall speed for one composition only, leading to a pair of intrinsic diffusion coefficients in a binary alloy. Therefore, few values of intrinsic diffusion coefficients have been recorded at high temperatures and on a limited range of the alloy composition. Moreover, experiments such as those by Anthony happened to be feasible in some Al, Cu, and Ag dilute alloys. As a result, a complete characterization of the L-coefficients of a specific concentrated alloy (even limited to the vacancy mechanism) has, to our knowledge, never been achieved. In the case of the interstitial diffusion mechanism, the tracer diffusion measurements under irradiation were not very convincing and did not lead to interstitial diffusion data. The interstitial data, which could be used in RIS models,[12] were the effective migration energies deduced from resistivity recovery experiments.

1.18.3.4 Determination of the Fluxes from Atomic Models

First-principles methods are now able to provide us with accurate values of jump frequencies in alloys, not only for the vacancy, but also for the interstitial in the split configuration (dumbbell). Therefore, an appropriate solution to estimate the L-coefficients is to start from an atomic jump frequency model for which the parameters are fitted to first-principles calculations.

1.18.3.4.1 Jump frequencies

In the framework of thermally activated rate theory, the exchange frequency between a vacancy V and a neighboring atom A is given by:

$$\Gamma_{AV} = \nu_{AV} \exp\left(-\frac{\Delta E_{AV}^{mig}}{k_B T}\right) \qquad [21]$$

if the activation energy (or migration barrier) ΔE_{AV}^{mig} is significantly greater than thermal fluctuations $k_B T$ (a similar expression holds for interstitial jumps). ΔE_{AV}^{mig} is the increase in the system energy when the A atom goes from its initial site on the crystal lattice to the saddle point between its initial and final positions. One of the key points in the kinetic studies is the description of these jump frequencies and of their dependence on the local atomic configuration, a description that encompasses all the information on the thermodynamic and kinetic properties of the system.

1.18.3.4.1.1 Ab initio calculations

In the last decade, especially since the development of the density functional theory (DFT), first-principle methods have dramatically improved our knowledge of point defect and diffusion properties in metals.[69] They provide a reliable way to compute the formation and binding energies of defects, their equilibrium configuration and migration barriers, the influence of the local atomic configuration in alloys, etc. Migration energies are usually computed by the drag method or by the nudged elastic band methods. The DFT studies on self-interstitial properties – for which few experimental data are available – are of particular interest and have recently contributed to the resolution of the debate on self-interstitial migration mechanism in α-iron.[70,71] However, the knowledge is still incomplete; calculations of point defect properties in alloys remain scarce (again, especially for self-interstitials), and, in general, very little is known about entropic contributions. Above all, DFT methods are still too time consuming to allow either the 'on-the-fly' calculations of the migration barriers, or their prior calculations, and tabulation for all the possible local configurations (whose

number increases very rapidly with the range of interactions and the number of chemical elements). More approximate methods are still required, based on parameters which can be fitted to experimental data and/or *ab initio* calculations.

1.18.3.4.1.2 Interatomic potentials

Empirical or semiempirical interatomic potentials, currently developed for molecular dynamics simulations, can be used for the modeling of RIS, but two problems must be overcome:

- To get a reliable description of an alloy, the interatomic potential should be fitted to the properties that control the flux coupling of point defects and chemical elements. A complete fitting procedure would be very tedious and, to our knowledge, has never been achieved for a given system.
- The direct calculation of migration barriers with an interatomic potential, even though much simpler than DFT calculations, is still quite time consuming. Full calculations of vacancy migration barriers have indeed been implemented in Monte Carlo simulations,[72] using massively parallel calculation methods, but they are still limited to relatively small systems and short times, for example, for the study of diffusion properties rather than microstructure evolution. It is possible to simplify the calculation of the jump frequency, for example, by not doing the full calculation of the attempt frequencies (their impact on the jump frequency must be less critical than that of the migration barriers involved in the exponential term) or by the relaxation of the saddle-point position.[73] Malerba *et al.* have recently proposed another method where the point defect migration barriers of an interatomic potential are exactly computed for a small subset of local configurations, the others being extrapolated using artificial intelligence techniques. This has been successfully used for the diffusion of vacancies in iron–copper alloys.[74,75] Such techniques have not yet been used to model RIS phenomena, but this could change in the future.

1.18.3.4.1.3 Broken-bond models

Because of these difficulties, simulations of diffusive phase transformation kinetics are commonly based on various broken-bond models, in the framework of rigid lattice approximations.[5,76] The total energy of the system is considered to be a sum of constant pair interaction energies, for example, $\varepsilon_{AB}^{(n)}$ between A and B atoms located on nth nn sites. Interactions between atoms and point defects can also be used to provide a better description of their formation energies and interactions with solute atoms, and other defects.

Various approximations are used to compute the migration barriers: a common one[77] is writing the saddle-point energy of the system as the mean energy between the initial energy E_i and final energy E_f, plus a constant contribution Q (which can depend on the jumping atom, A or B). The migration barrier for an A–V exchange is then:

$$\Delta E_{AV}^{mig} = \frac{E_f - E_i}{2} + Q_A \qquad [22]$$

where $E_f - E_i$ corresponds to the balance of bonds destroyed and created during the exchange.

Another solution is to explicitly consider the interaction energy e_{AV}^{SP} of the jumping atom A with the system, when it is at the saddle point:

$$\Delta E_{AV}^{mig} = e_{AV}^{SP} - \sum_{i,n} \varepsilon_{Ai}^{(n)} - \sum_{j,n} \varepsilon_{Vj}^{(n)} \qquad [23]$$

e_{AV}^{SP} itself can be written as a sum of interactions between A and the neighbors of the saddle point.[12,78,79]

Both approximations are easily extended to interstitial diffusion mechanisms, and their parameters can be fitted to experimental data and/or *ab initio* calculations. The first one has the drawback of imposing a linear dependence between the barrier and the difference between the initial and final energies, which is not justified and has been found to be unfulfilled in the very few cases where it has been checked[72] (with empirical potentials). The second one should better take into account the effect of the local configuration and, according to the theory of activated processes, does not impose a dependence of the barrier on the final state. However, a model of pair interactions on a rigid lattice does not give a very precise description of the energetic landscape in a metallic solid solution, so, the choice of approximations [22] or [23] may not be crucial. Taking into account many-body interactions (fitted to *ab initio* calculations, using cluster expansion methods) could improve the description of migration barriers, but would significantly increase the simulation time.[80,81]

1.18.3.4.2 Calculation of the phenomenological coefficients

Given an atomic jump frequency model, transitions of the alloy configurations are described by a master equation. With one point defect in the system, a Monte Carlo simulation produces a trajectory of the

alloy in the configuration space. The L-coefficients can be obtained from a Monte Carlo simulation. Measurements are performed on an equilibrated system using the generalized Einstein formula of Allnatt.[82] This numerical approach has proved its efficiency; however, the achievement of a predictive model using this method is limited to short ranges of composition and temperature. Simulations become rapidly unworkable when, for example, binding energies between interstitials and neighboring atoms are significant.[9,83] The simulated trajectory can be trapped in some configurations due to the correlation effects of the diffusion mechanism; after a jump, an atom has a finite probability to exchange again with the same point defect and cancel its first jump. The escape probability of the point defect from an atom decreases with the binding energy between the two species.

In the limited case of dilute alloys in which a few point defect jump frequencies are involved, it is possible to consider all the vacancy paths and deduce analytical expressions for the L-coefficients. On the other hand, diffusion models of concentrated alloys lead to approximate expressions of the transport coefficients.

1.18.3.4.2.1 Dilute alloys

The point defect jump frequencies to be considered are those that are far from the solute, those leaving the solute, those arriving at a nn site of the solute, and those jumping from nn to nn sites of the solute. Diffusivities are approached by a series in which the successive terms include longer and longer looping paths of the point defect from the solute. Using the pair-association method, the whole series has been obtained for the vacancy mechanism in body-centered cubic (bcc) and face-centered cubic (fcc) binary alloys with nn interactions (cf. Allnatt and Lidiard[6] for a review). However, there is still no accurate model for the effect of a solute atom on the self-diffusion coefficient.[84] The L-coefficients as well as the tracer diffusivities depend on three jump frequency ratios in the fcc structure and two ratios in the bcc structure. For the irradiation studies, the same pair-association method has been applied to estimate the L-coefficients of the dumbbell diffusion mechanism in fcc[85,86] and bcc[83,87] alloys. Note, that the pair-association calculation in bcc alloys[87] has recently been improved by using the self-consistent mean-field (SCMF) theory.[83] The calculation includes the effect of the binding energy between a dumbbell of solvent atoms and a solute.

In the case of the vacancy diffusion mechanism, before the development of first-principles calculation methods, reliable jump frequency ratios could be estimated from a few experimental diffusion coefficients (three for fcc and two for bcc). Data were calculated from the solvent and solute tracer diffusivities, the linear enhancement of self-diffusion with solute concentration, or the electro-migration enhancement factors of tracer atoms in an electric field.[88] Some examples of jump frequency ratios fitted to experimental data are displayed in tables.[89] Currently, the most widely used approach is using first-principles calculations to calculate not only the vacancy, but also the interstitial jump frequencies.

1.18.3.4.2.2 Concentrated alloys

The first diffusion models devoted to concentrated alloys were based on a very basic description of the diffusion mechanism. The alloy is assimilated into a random lattice gas model where atoms do not interact and where vacancies jump at a frequency that depends only on the species they exchange with (two frequencies in a binary alloy). Using complex arguments, Manning[8] could express the correlation factors as a function of the few jump frequencies. The approach was extended to the interstitial diffusion mechanism.[90] At the time, no procedure was suggested to calculate these mean jump frequencies from an atomic jump frequency model. Such diffusion models, which consider a limited number of jump frequencies, already make spectacular correlation effects appear possible, such as a percolation limit when the host atoms are immobile.[8,91,92] But they do not account for the effect of short-range order on the L-coefficients although one knows that RIS behavior is often explained by means of a competition between binding energies of point defects with atomic species, especially in dilute alloys. Some attempts were made to incorporate short-range order in a Manning-type formulation of the phenomenological coefficients, but coherency with thermodynamics was not guaranteed.[93,94]

The current diffusion models, including short-range order, are based on either the path probability method (PPM)[95–97] or the SCMF theory.[84,92,98–100] Both mean-field methods start from an atomic diffusion model and a microscopic master equation. While the PPM considers transition variables, which are deduced from a minimization of a pseudo free-energy functional associated to the kinetic path, the SCMF theory introduces an effective Hamiltonian to represent the nonequilibrium correction to the

distribution function probability and calculates the effective interactions by imposing a self-consistent constraint on the kinetic equations of the distribution function moments. Diffusion models built from the PPM were developed in bcc solid solution and ordered alloys, using nn pair transition variables, which is equivalent to considering nn effective interactions, and a statistical pair approximation for the equilibrium averages within the SCMF theory.[95,96] The SCMF theory extended the approach to fcc alloys[8,91,92] and provided a model of the composition effect on solute drag by vacancies.[98] The interstitial diffusion mechanism was also tackled.[10,83,101] For the first time, an interstitial diffusion model including short-range order was proposed in bcc concentrated alloys.[10] It was shown that the usual value of 1 eV for the binding energy of an interstitial with a neighboring solute atom leads to very strong effects on the average interstitial jump frequency and, therefore, on the L-coefficients.

1.18.4 Continuous Models of RIS

RIS is a phenomenon that couples the fluxes of defects created by irradiation and the alloy components. In RIS models, point defect diffusion mechanisms alone are considered, although it is accepted that displacement cascades produce mobile point defect clusters, which may contribute to the RIS. In the first section, we present the expressions used to simulate the RIS, the main results, and limits. Some examples of application to real alloys are discussed in the second part. The last section suggests some possible improvements in the RIS models.

1.18.4.1 Diffusion Models for Irradiation: Beyond the TIP

RIS models have two main objectives: (1) to describe the reaction of a system submitted to unusual driving forces, such as point defect concentration gradients; and (2) to reproduce the atomic diffusion enhancement induced by an increase of the local point defect concentration. In comparison with the thermal aging situation, gradients of point defect chemical potential are nonnegligible. The L-coefficients are considered as variables that vary with nonequilibrium point defect concentrations. With L-coefficients varying in time, such models do not satisfy the TIP hypothesis. Instead, the authors of the first publications[11,30,102] considered new quantities, the so-called partial diffusion coefficients, as new constants associated with a temperature and a nominal alloy composition. The first authors to express the partial diffusion coefficients in terms of the L-coefficients were Howard and Lidiard[103] for the vacancy in dilute alloys, Barbu[86] for the interstitial in dilute alloys, and Wolfer[11] in concentrated alloys. In the following, we use the formulation of Wolfer because the approximations made to calculate the L-coefficients and driving forces are clearly stated. In a binary alloy (AB), fluxes are separated into two contributions: the first one induced by the point defect concentration gradients, and the second one appearing after the formation of chemical concentration gradients near the point defect sink[11]:

$$\begin{aligned}
\mathcal{J}_A &= -(d^c_{AV} C_V + d^c_{AI} C_I)\Phi \nabla C_A + C_A (d_{AV} \nabla C_V - d_{AI} \nabla C_I) \\
\mathcal{J}_V &= -(C_A d_{AV} + C_B d_{BV}) \nabla C_V + C_V \Phi (d^c_{AV} \nabla C_A + d^c_{BV} \nabla C_B) \\
\mathcal{J}_I &= -(C_A d_{AI} + C_B d_{BI}) \nabla C_I - C_I \Phi (d^c_{AI} \nabla C_A + d^c_{BI} \nabla C_B)
\end{aligned} \quad [24]$$

with partial diffusion coefficients defined in terms of the L-coefficients and the equilibrium point defect concentration

$$\begin{aligned}
d_{AV} &= \frac{L^V_{AA} + L^V_{AB}}{C_A C_V}, \quad d_{AI} = \frac{L^I_{AA} + L^I_{AB}}{C_A C_I} \\
d^c_{AV} &= \frac{L^V_{AA}}{C_A C_V} - \frac{L^V_{AB}}{C_B C_V} + d_{AV} \frac{1}{\Phi} \zeta_{VA} \\
d^c_{AI} &= \frac{L^I_{AA}}{C_A C_I} - \frac{L^I_{AB}}{C_B C_I} - d_{AI} \frac{1}{\Phi} \zeta_{IA}
\end{aligned} \quad [25]$$

where ζ_{VA} is defined in terms of the local equilibrium vacancy concentration (see eqn [14]). Flux of B is deduced from the flux of A by exchanging the letters A and B. In a multicomponent alloy, equivalent kinetic equations are provided by Perks's model.[104] In this model, point defect concentrations are assumed to be independent of chemical concentrations: in other words, parameters ζ_{VA} and ζ_{VB} are set to zero. Most of the RIS models are derived from Perks' model although they neglect the cross-coefficients.[5] Flux of species i is assumed to be independent of the concentration gradients of the other species. In doing so, not only the kinetic couplings, but also some of the thermodynamic couplings are ignored. Indeed, as shown in eqn [9], a chemical potential gradient is a function of all the concentration gradients.

An atomic flux results from a balance between the so-called IK effect, atomic fluxes induced by point defect concentration gradients (first term of the RHS of eqn [24]), and the so-called Kirkendall (K) effect

reacting against the formation of chemical concentration gradients at sinks produced by the IK effect (last term of LHS of eqn [24]). Equation [24] can be used in both dilute and concentrated alloys. Differences between models arise when one evaluates specific partial diffusion coefficients.

The first RIS model in dilute fcc alloys, designed by Johnson and Lam,[105] introduced an explicit variable for solute–point defect complexes. The same kind of approach has been used by Faulkner *et al.*,[106] although it has been shown to be incorrect in specific cases.[86,107] A more rigorous treatment relies on the linear response theory, with a clear correspondence between the atomic jump frequencies and the L-coefficients. The first RIS model derived from a rigorous estimation of fluxes was devoted to fcc dilute alloys,[108] and then to bcc dilute alloys.[87]

In concentrated alloys, due to the greater complexity and the lack of experimental data, further simplifications and more approximate diffusion models are used to simulate RIS.

1.18.4.1.1 Manning approximation

In **Section 1.18.3.3**, we mentioned the difficulty in measuring the L-coefficients of an alloy, especially those involved in fluxes induced by point defect concentration gradients. Diffusion data are even more difficult to obtain for the interstitials. This is probably why most of the RIS models emphasize the effect of vacancy fluxes, with the interstitial contribution assumed to be neutral.

The first model proposed by Marwick[30] introduced the main trick of the RIS models by taking out vacancy concentration as a separate factor of the diffusion coefficients. Expressions of the fluxes were obtained using a basic jump frequency model, which is equivalent to neglecting the cross-terms of the Onsager matrix. According to the random lattice gas diffusion model of Manning,[8] correlation effects are added as corrections to the basic jump frequencies. The resulting fluxes[30] are similar to eqn [24], except that the c-partial diffusion coefficients (d^{c}_{AV}, d^{c}_{AI}) are now equal to the partial diffusion coefficients (d_{AV}, d_{AI}), which is equivalent to neglecting cross L-coefficients and the dependence of equilibrium point defect concentration on alloy composition. However, for the first time, the segregation of a major element, Ni, in concentrated austenitic steel was qualitatively understood in terms of a competition between fast- and slow-diffusing major alloy components.

The partial diffusion coefficients associated with the vacancy mechanism are estimated using the relations of Manning, deducing the L-coefficients from the tracer diffusion coefficients:

$$L^{V}_{ij} = C_i D^{*}_i \left[\delta_{ij} + \frac{1 - f_0}{f_0} \frac{C_j D^{*}_j}{\sum_k C_k D^{*}_k} \right] \qquad [26]$$

One observes that the Manning[8] relations systematically predict positive partial diffusion coefficients:

$$d_{\alpha V} = D^{*}_{\alpha} / C_V \qquad [27]$$

Moreover, the three L-coefficients of a binary alloy are no longer independent. Both constraints are known to be catastrophic in dilute alloys, while they seem to be capable of satisfactorily describing RIS of major alloy components in austenitic steels.[30]

1.18.4.1.2 Interstitials

Wiedersich *et al.*[102] added to Marwick's model a contribution of the interstitials. The global interstitial flux is described by eqn [24], while preferential occupation of the dumbbell by a species or two is deduced from the alloy concentration and the effective binding energies. Such a local equilibrium assumption implies very large interstitial jump frequencies compared to atomic jump frequencies. This kind of model yields an analytical description of stationary RIS (see below eqn [28]). An explicit treatment of the interstitial diffusion mechanism was also investigated. From a microscopic description of the jump mechanism, one derives the kinetic equations associated with each dumbbell composition.[109–112] Unlike previous models, there is no local equilibrium assumption, but correlation effects are neglected (except in Bocquet[90]). They could have used the interstitial diffusion model with the correlations of Bocquet.[90] However, due to the lack of data for the interstitials, most of the recent concentrated alloy models neglect the interstitial contribution to RIS.[104,113,114]

1.18.4.1.3 Analytical solutions at steady state

An analytical solution of the coupled equations is obtained within steady-state conditions.[102] At the boundary plane, variation of composition is controlled by a unique flux coming from the bulk. A steady-state condition implies that the latter flux is zero, and that, step by step, every flux is zero. In a binary alloy, eqn [24] leads to a relationship between concentration gradients[102]:

$$\nabla C_A = \frac{C_A C_B d_{BI} d_{AI}}{(C_B d_{BI} D_A + C_A d_{AI} D_B)} \left(\frac{d_{AV}}{d_{BV}} - \frac{d_{AI}}{d_{BI}} \right) \nabla C_V \qquad [28]$$

where the intrinsic diffusion coefficient is equal to $D_\alpha = (d^c_{\alpha V} C_V + d^c_{\alpha I} C_I)\Phi$. The spatial extent of segregation coincides with the region of nonvanishing defect gradients. Note that, in the original paper,[102] the partial and c-partial diffusion coefficients were taken to be equal. Such a simplification may change the amplitude of the RIS predictions. In a multicomponent alloy, not only the amplitude, but also the sign of RIS might be affected by this simplification. In dilute alloys, the whole kinetics can be approached by an analytical equation as long as the Kirkendall fluxes resulting from the formation of RIS are neglected.[115]

1.18.4.1.4 Concentration-dependent diffusion coefficients

Most of the RIS models assume thermodynamic factors equal to 1, although in the first paper,[11] a strong variation was observed between the thermodynamic factor and composition. Similarly, the quantities $\zeta_{V\alpha}$ and $\zeta_{I\alpha}$ of the point defect driving forces [14] are expected to depend on local concentration and stress field.[11,116] For example, Wolfer[11] demonstrated that RIS could affect the repartition between interstitial and vacancy fluxes and thereby, the swelling phenomena. The bias modification might be due to several factors: a Kirkendall flux induced by the RIS formation, or the dependence of the point defect chemical potentials on local composition, including the elastic and chemical effects.

A local-concentration-dependent driving force is due to the local-concentration-dependent atomic jump frequencies. Following this idea, the modified inverse Kirkendall (MIK) model introduces partial diffusion coefficients of the form[113]

$$d_{AV} = d^0_{AV} \exp\left(\frac{-E^m_{AV}}{k_B T}\right) \qquad [29]$$

The migration energy is written as the difference between the saddle-point energy and the equilibrium energy. It depends on local composition through pair interactions calculated from thermodynamic quantities such as cohesive energies, vacancy formation energies, and ordering energies. In fact, the present partial diffusion coefficients correspond to a mesoscopic quantity deduced from a coarse-grained averaging of the microscopic jump frequencies. In principle, not only the effective migration energies, but also the mesoscopic correlation coefficients and thermodynamic factors should depend on local concentrations. Nevertheless, the thermodynamic factors, correlation coefficients, and the $\zeta_{V\alpha}$ factor are assumed to be those of the pure metal A. Recently, a new continuous model suggested a multifrequency formulation of the concentration-dependent partial diffusion coefficients. Instead of averaging the sums of interaction bonds in the exponential argument, every jump frequency corresponding to a given configuration is considered with a configuration probability weight.[17] Predictions of the model are compared with direct RIS Monte Carlo simulations that rely on the same atomic jump frequency models. In the two presented examples, the agreement is satisfactory. However, the thermodynamic factor and correlation coefficients are yet to be defined clearly.[17]

1.18.4.2 Comparison with Experiment

1.18.4.2.1 Dilute alloy models

RIS measurements in dilute alloys are less numerous than in concentrated alloys because the required grain boundary concentrations are usually smaller. However, some of the first RIS observations concerned the segregation of a dilute element, Si, in austenitic steels. In this specific case, observations were easy because the RIS of Si was accompanied by precipitation of Ni_3Si.

The first mechanism that was proposed to explain the observed solute segregation was the diffusion of solute–point defect complexes towards sinks.[105] Since then, more rigorous models that rely on the linear response theory have been established and applied to the RIS description of Mn and P in nickel[108] and P in ferritic steels.[87,107] Although good precision of the microscopic parameters was still missing, the formulation of the kinetic equations was general enough to be used almost without modification.[105] Recent *ab initio* calculations not only provided accurate atomic jump frequencies of P in Fe,[7,70] but they also called into question the jump interstitial diffusion mechanism that had to be considered.[7] Indeed, the octahedral and the (110) mixed dumbbell configurations have almost the same stability and migration enthalpies. The resulting effective diffusion energy estimated by the transport model was found to be smaller than the self-interstitial atom migration enthalpy, confirming the classical statement that a solute atom with a negative size effect tends to segregate at the grain boundary. However, as emphasized in Meslin *et al.*,[7] the current interpretation of the interstitial contribution to RIS in terms of size effects is certainly oversimplified. A very large *ab initio* value of 1.05 eV for the binding energy between a mixed dumbbell and a substitutional P atom may lead to a large activation energy for P interstitials and a drastic reduction of P segregation predictions.[7] To consider

this new blocking configuration with two P atoms, a concentrated alloy diffusion model including short-range-order effects is required.

It is interesting to note that the same solute seems to have a positive coupling with the vacancy also (although the calculation was not as precise as for the interstitials as it was based on an empirical potential).[117] In the same way, recent *ab initio* calculations showed that a Cu solute is also expected to be dragged by vacancy at low temperatures in Fe.[118,119]

1.18.4.2.2 Austenitic steels

Most of the RIS models for concentrated alloys were devoted to the ternary Fe–Cr–Ni system, which is a model alloy of austenitic steels. The diffusion ratios used in the fitting process are the ones extracted from the tracer diffusion coefficients measured by Rothman *et al.* (referenced in Perks and Murphy[104] and Allen and Was[113]). In most of the studies, the input parameters are taken from Perks model.[104] The more recent MIK model, which was initially based on the Perks model, used the CALPHAD database to fit its concentration-dependent migration energy model.[113] A significant improvement in the predictive capabilities of RIS modeling was concluded after a systematic comparison with RIS, observed by Auger spectroscopy in Fe–Cr–Ni as a function of temperature, nominal composition, and irradiation dose.[113] However, all the models were proved to be powerful enough to reproduce the correct tendencies of RIS in austenitic steels: a depletion of Cr and an enrichment of Ni near a grain boundary. When the binding energies of point defects with atoms are not so strong and the ratios between the tracer diffusion coefficients of the major elements are large enough (larger than 2–3), a rough estimation of the partial diffusion coefficients from tracer diffusion coefficients seems to be sufficient to reproduce the main tendencies.

The interstitial contribution to RIS is usually neglected due to the lack of diffusion data. Stepanov *et al.*[120] observed an electron-irradiated foil at a temperature low enough so that only interstitials contributed to the RIS. Segregation profiles were similar to the typical ones at higher temperature. Parameters of the interstitial diffusion model were estimated in such a way that the experimental RIS was reproduced. The migration energy of interstitials was assumed to be equal to 0.2 eV, which is quite low in comparison with the effective migration energy deduced from recovery resistivity measurements.[121]

The attempts of the MIK model to reproduce the characteristic 'W-shaped' Cr profiles observed at intermediate doses were not conclusive[36]; transitory profiles disappeared after a dose of 0.001 dpa, while the experimental threshold value was around 1 dpa. A possible explanation may be the approximation used to calculate the chemical driving force. Indeed, a thermodynamic factor equal to 1 pushes the system to flatten the concentration profile in reaction to the formation of the RIS profile. A study based on a lattice rate theory pointed out that an oscillating profile was the signature of a local equilibrium established between the surface plane and the next plane.[13] This kind of mean-field model predicts that the local enrichment of Cr at a surface persists at larger irradiation dose (0.1 dpa), though not as large as the experimental value.

The role of impurities as point defect traps has been explored since the 1970s.[122] In those models, impurities do not contribute to fluxes but to the sink population as immobile sinks with an attachment parameter depending on an impurity–point defect binding energy.[123] Other models account for immobile vacancy traps by renormalizing the recombination coefficient with a vacancy–impurity binding energy.[120] Whether by vacancy or by interstitial trapping, the result is a recombination enhancement and a decrease of point defect concentrations, leading to a reduction of RIS and swelling. Hackett *et al.*[123] estimated some binding energies between a vacancy and impurities, such as Pt, Ti, Zr, and Hf in fcc Fe, using *ab initio* calculations. The energy calculations seem to have been performed without relaxing the structure, probably because fcc Fe is not stable at 0 K. Although the absolute values of the binding energies should be used with caution, one can expect the strong difference between the binding energies of a vacancy with Zr (1.08 eV) and Hf (0.71 eV) to persist after a relaxation of atomic positions. In a more rigorous way, the trapping of dumbbells could be modeled using the high migration energy associated with dumbbells bound to an impurity.[12] Such a model would allow the impurity to migrate and change the sink density with dose. The same model could explain the recent experimental results observing that, after a few dpa, RIS of the major elements starts again.[123]

RIS in austenitic steels was observed to be strongly affected by the nature of the grain boundary, that is, by the misorientation angle and the Σ value.[40] Differences between the observed RIS are explained by a so-called grain boundary efficiency, introduced in a modified rate equation model.[40,109,114,124] Calculations of vacancy formation energies at different

grain boundaries, for example, in nickel in which atomic interactions are described by an embedded atom method, have been used to model sink strength as a function of misorientation angle. The resulting RIS predictions around several tilt grain boundaries were found to be in good agreement with RIS data.[124] Grain boundary displacement and its effect on RIS were considered too. Grain boundary displacement was explained by an atomic rearrangement process due to recombination of excess point defects at the interface. New kinetic equations including an atomic rearrangement process after recombination of point defects at the interface predict asymmetrical concentration profiles, in agreement with experiments.[114]

1.18.4.3 Challenges of the RIS Continuous Models

Ab initio calculations have become a very powerful tool for RIS simulations. They have been shown to be able to provide not only the variation of the atomic jump frequencies with local concentration,[125] but also new diffusion mechanisms.[7] From a precise knowledge of the atomic jump frequencies and the recent development of diffusion models,[98] a quantitative description of the flux coupling is expected to be feasible even in concentrated alloys. A unified description of flux coupling in dilute and concentrated alloys would allow the simultaneous prediction of two different mechanisms leading to RIS: solute drag by vacancies, and an IK effect involving the major elements.

An RIS segregation profile spreads over nanometers. Cell sizes of RIS continuous models are then too small for the theory of TIP to be valid. A mesoscale approach that includes interface energy between cells, such as the Cahn–Hilliard method, would be more appropriate. A derivation of quantitative phase field equations with fluctuations has recently been published.[62] The resulting kinetic equations are dependent on the local concentration and also cell-size dependent. However, the diffusion mechanism involved direct exchanges between atoms. The same method needs to be developed for a system with point defect diffusion mechanisms.

Although it has been suggested since the first publications[30] that the vacancy flux opposing the set up of RIS could slow down the void swelling, the change of microstructure and its coupling with RIS have almost never been modeled. Only very recently, phase field methods have tackled the kinetics of a concentration field and its interaction with a cavity population (see **Chapter 1.15, Phase Field Methods**). The development of a simulation tool able to predict the mutual interaction between the point defect microstructure and the flux coupling is quite a challenge.

1.18.5 Multiscale Modeling: From Atomic Jumps to RIS

The knowledge of the phenomenological coefficients L, including their dependence on the chemical composition, allows the prediction of RIS phenomena. Unfortunately, in practice, it is very difficult to get such information from experimental measurements, especially for concentrated and multicomponent alloys, and for the diffusion by interstitials. As we have seen, it is also quite difficult to establish the exact relationship between the phenomenological coefficients and the atomic jump frequencies because of the complicated way in which they depend on the local atomic configurations and because correlation effects are very difficult to be fully taken into account in diffusion theories. An alternative approach to analytical diffusion equations, then, is to integrate point defect jump mechanisms, with a realistic description of the frequencies in the complex energetic landscape of the alloy, in atomistic-scale simulations such as mean-field equations, or Monte Carlo simulations (molecular dynamics methods are much too slow – by several orders of magnitude – for microstructure evolution governed by thermally activated migration of point defects).

Atomic-scale methods are appropriate techniques to simulate nanoscale phenomena like RIS. They are all based on an atomic jump frequency model. From this point of view, the difficulties are the same as for the modeling of other diffusive phase transformations (such as precipitation or ordering during thermal aging), complicated by the point defect formation and annihilation mechanisms and by the self-interstitial jump mechanisms, which are usually more complex than the vacancy ones.[76]

1.18.5.1 Creation and Elimination of Point Defects

Because RIS is due to fluxes of excess point defects, modeling must take into account their creation and elimination mechanisms. It must, for example, reproduce the ratio between vacancy and interstitial concentrations that controls the respective weights of annihilation by recombination or elimination at sinks. The situation from this point of view is very different from phase transformations during thermal

aging, where usually only vacancy diffusion occurs, and simulations can be performed with nonphysical point defect concentrations and a correction of the timescale (see, e.g., Le Bouar and Soisson[78] and Soisson and Fu[125]).

During electron or light ion irradiation, defects are homogeneously created in the material, with a frequency directly given by the radiation flux (in dpa s^{-1}), a condition that is easily modeled in continuous models, mean-field models,[12,14] or Monte Carlo simulations.[16,118] The formation of defects in displacement cascades during irradiation by heavy particles can also be introduced in kinetic models, using the point defect distributions computed by molecular dynamics.[126] The annihilation mechanisms at sinks such as surfaces or grain boundaries are, for the time being, simulated using very simple approximations (perfects sinks, no formation/annihilation of kinks on dislocations, or steps on surfaces). This should not affect the basic coupling between diffusion fluxes, but the long-term evolution of the sink microstructure – which will eventually have an impact on the chemical distribution – cannot be taken into account.

Finally, thermally activated point defect formation mechanisms that operate during thermal aging, are taken into account in some simulations.[11–14] Simulations that do not include the thermal production are then valid only at sufficiently low temperatures, when defect concentrations under irradiation are much larger than equilibrium ones.

1.18.5.2 Mean-Field Simulations

The first mean-field lattice rate models included two thermally activated jump frequencies, one for the vacancy and the other for the interstitial. A direct interstitial diffusion mechanism[14] and later a dumbbell diffusion mechanism[12] have been modeled in detail. The vacancy jump frequency parameters are fitted to available thermodynamic and tracer diffusion data, and the interstitial parameters are fitted to effective migration energies derived from resistivity recovery measurements.[121] The resulting local-concentration-dependent jump frequencies describe both the kinetics of thermal alloys toward equilibrium and irradiation-induced surface segregation in concentrated alloys. The surface and its vicinity are modeled by the stacking of N parallel atomic planes perpendicular to the diffusion axis, which is taken to be a [100] direction of an fcc alloy. A mirror boundary condition is used at one end, and a free surface, which can act as both a source and sink for point defects at the other end. Above the surface, a buffer plane almost full of vacancies is added. Fluxes between the buffer plane and vacuum are forbidden. The resulting equilibrium segregation profiles are controlled by the nominal composition, temperature, and two interaction contributions, the first one expressed in terms of the surface tensions and the second in terms of the ordering energies. Note, that the predicted equilibrium vacancy concentration at the surface is much higher than in the bulk.

Time dependence of mean occupations in an atomic plane of point defects and atoms results from a balance between averaged incoming and outgoing fluxes. Fluxes are written within a mean-field approximation, decoupling the statistical averages into a product of mean occupations and mean jump frequencies for which the occupation numbers in the exponential argument are replaced by the corresponding mean occupations. The resulting first order differential kinetic equations are integrated using a predictor corrector variable time step algorithm because of the high jump frequency disparities between vacancies and interstitials.

It is observed that interstitial contribution to RIS is of the same order as that of the vacancy. The predicted formation of a 'W-shaped' profile as a transient state from the preirradiated enrichment to the strong depletion of Cr is shown to be governed by both thermodynamic properties and the relative values of the transport coefficients between Fe, Cr, and Ni (**Figure 9**). Thermodynamics not only plays a part in the transport coefficients but also arises in the establishment of a local equilibrium between the surface and the adjacent plane, explaining the oscillatory behavior of the Cr profile: an equilibrium tendency toward an enrichment of Cr at the grain boundary plane, which competes with a Cr depletion tendency under irradiation. However, the predicted profile is not as wide as the experimental one.

What needs to be improved is the interstitial diffusion model. The lack of experimental and *ab initio* data leads to approximate interstitial jump frequencies. Coupling between fluxes is described partially as correlation effects are not accounted for. The recent mean-field developments[98] should be integrated in this type of simulation.

1.18.5.3 Monte Carlo Simulations

AKMC simulations can be used to follow the atomic configuration of a finite-sized system, starting from a given initial condition, by performing successive

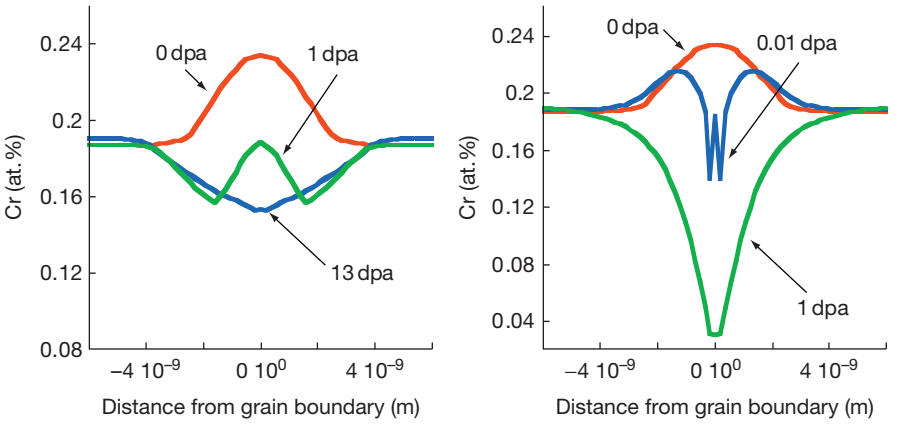

Figure 9 Comparison of Cr segregation profiles as a function of irradiation dose in FeNi12Cr19 at $T = 635$ K. Left cell represents typical experimental results of Busby *et al.*,[36] right cell is mean-field predicted result starting from the experimental profile observed just before irradiation. Reproduced from Nastar, M. *Philos. Mag.* **2005**, *85*, 641–647.

point defect jumps.[16,17,126,127] Then, the migration barriers are exactly computed (in the framework of the used diffusion model) for each atomic configuration using equations such as [22] or [23], without any mean-field averaging. The jump to be performed can be chosen with a residence time algorithm,[128,129] which can also easily integrate creation and annihilation events.[16]

Correlation effects between successive point defect jumps, as well as thermal fluctuations, are naturally taken into account in AKMC simulations; this provides a good description of diffusion properties and of nucleation events (the latter being especially important for the modeling of RIP). The downside is that they are more time consuming than mean-field models, especially when correlation or trapping effects are significant. These advantages and drawbacks explain why AKMC is especially useful to model the first stages of segregation and precipitation kinetics.

AKMC simulations were first used to study RIS and RIP in model systems,[16,17] to highlight the control of segregation by point defect migration mechanism, and to test the results of classical diffusion equations. These studies show that it is possible – in favorable situations, where correlation and trapping effects are not too strong – to simulate microstructure evolution with realistic dose rates and point defect concentrations, up to doses of typically 1 dpa.

In simple cases, AKMC simulations can validate the predictions of continuous models, on the basis of simple diffusion equations[17,16]: an example is given in **Figure 10** for an ideal solid solution, that is, when RIS can be studied without any clustering or ordering tendency.[16] In this simulation, the diffusion of A atoms by vacancy jumps is more rapid than that of B atoms, and one observes an enrichment of B atoms at the sinks due to the IK effect (A and B atoms diffuse at the same speed by interstitial jumps; those jumps therefore do not contribute to the segregation). One can notice the nonmonotonous shape of the concentration profile, which corresponds to the prediction of Okamato and Rehn[29] when the partial diffusion coefficients are $d_{BV}/d_{AV} < d_{BI}/d_{AI}$. In the more complicated case of a regular solution, Rottler *et al.*[17] have shown that the RIS profiles of AKMC simulations can be reproduced by a continuous model using a self-consistent formulation, which gives the dependence of the partial diffusion coefficients with the local composition.

In alloys with a clustering tendency, AKMC simulations have been used to study microstructure evolution when RIS and precipitation interact, either in under- or supersaturated alloys. The evolution of the precipitate distribution can be quite complicated as the kinetics of nucleation, growth, and coarsening depend on both the local solute concentrations and the point defect concentrations (which control solute diffusion), concentrations that evolve abruptly in the vicinity of the sinks.[16] A case of homogeneous RIP, due to a mechanism similar to the one proposed by Cauvin and Martin[52] (see **Section 1.18.2.4**), has been simulated with a simplified interstitial diffusion model.[130,131]

The application of AKMC to real alloys has just been introduced. Copper segregation and precipitation in α-iron has been especially studied, because of its role in the hardening of nuclear reactor pressure vessel steels.[118,126,127,132,133] These studies are based on rigid

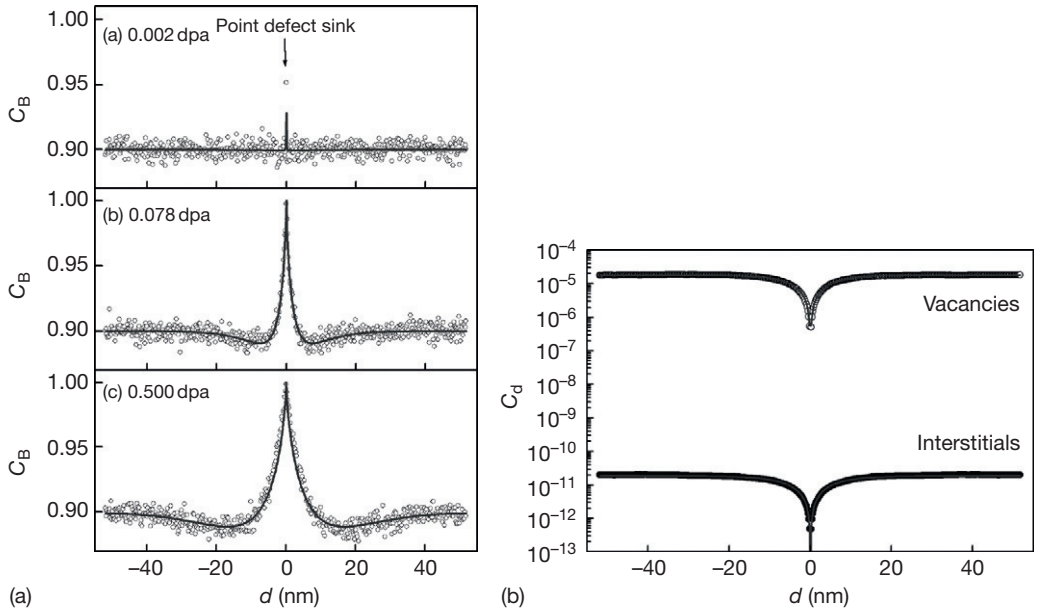

Figure 10 (a) Evolution of the B concentration profile in an $A_{10}B_{90}$ ideal solid solution under irradiation at 500 K and 10^{-3} dpa s^{-1}, when $d_{AV} > d_{BV}$ and $d_{Ai} = d_{Bi}$; (b) Point defect concentration profiles in the steady state. Reproduced from Soisson, F. *J. Nucl. Mater.* **2006**, 349, 235–250.

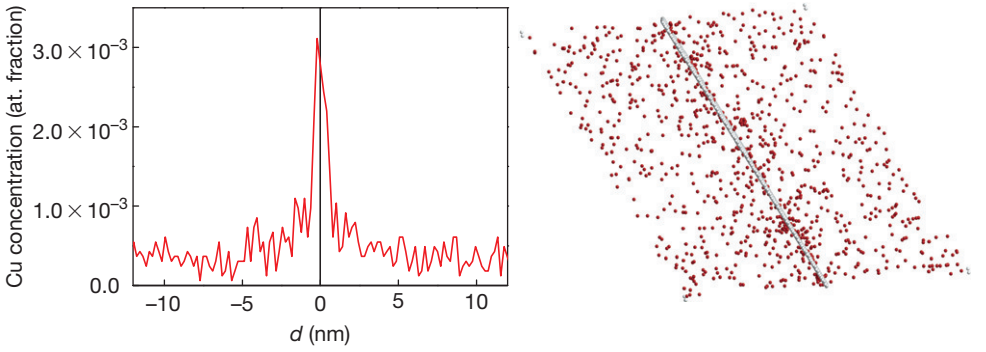

Figure 11 Concentration profile and formation of small copper clusters near a grain boundary, in a Fe–0.05%Cu alloy under irradiation at $T = 500$ K and $K_0 = 10^{-3}$ dpa s^{-1}.

lattice approximations, using parameters fitted to DFT calculations. The point defect formation energies are found to be much smaller in copper-rich coherent clusters than in the iron matrix,[79,118] and there is a strong attraction between vacancies and copper atoms in iron, up to the second-nearest neighbor positions.[70,125] AKMC simulations show that in dilute Fe–Cu alloys, the $L_{CuV} = -[L_{CuCu} + L_{CuFe}]$ is positive at low temperatures, because of the diffusion of Cu–V pairs. At higher temperatures, Cu–V pairs dissociate and L_{CuV} becomes negative.[118,119] The resulting segregation behaviors have been simulated, with homogeneous formation of Frenkel pairs (i.e., conditions corresponding to electron irradiations). Only vacancy fluxes are found to contribute to RIS; copper concentration increases near the sinks at low temperatures and decreases at high temperatures.[118] In highly supersaturated alloys, RIS does not significantly modify the evolution of the precipitate distribution, except for the acceleration proportional to the point defect supersaturation. Figure 11 illustrates a simulation of RIS in a very dilute Fe–Cu alloy, performed with the parameters of Soisson and Fu[118,125]; the segregation of copper at low temperatures produces the preferential formation of small copper-rich clusters near the sinks, which could correspond to the beginning of a

heterogeneous precipitation. However, simulations are limited to very short irradiation doses because of the trapping of defects as soon as the first clusters are formed. This makes it difficult to draw conclusions from these studies.

Coprecipitation of copper clusters with other solutes (Mn, Ni, and Si) has been modeled by Vincent *et al.*[126,127] and Wirth and Odette[133] under irradiation at very high radiation fluxes and with formation of point defects in displacement cascades. AKMC simulations display the formation of vacancy clusters surrounded by copper atoms, which could result both from the Cu–V attraction (a purely thermodynamic factor) and from the dragging of Cu by vacancies (effect of kinetic coupling). The formation of Mn-rich clusters is favored by the positive coupling between fluxes of self-interstitials and Mn (DFT calculations show that the formation of mixed Fe–Mn dumbbells is energetically favored).

1.18.6 Conclusion

We started this review with a summary of the experimental activity on RIS. Intensive experimental work has been devoted to austenitic steels and its model fcc alloys (Ni–Si, Ni–Cr, and Ni–Fe–Cr) and, more recently, to ferritic steels. A strong variation of RIS with irradiation flux and dose, temperature, composition, and the grain boundary type was observed. One study tried to take advantage of the sensitivity of RIS to composition to inhibit Cr depletion at grain boundaries. A small addition of large-sized impurities, such as Zr and Hf, was shown to inhibit RIS up to a few dpa in both austenitic and ferritic steels. On the other hand, the Cr depletion at grain boundaries was observed to be delayed when the grain boundary was enriched in Cr before irradiation. A 'W-shaped' transitory profile could be maintained until a few dpa before the grain boundary was depleted in Cr. The mechanisms involved in these recent experiments are still not well understood, although RIS model development was closely related to the experimental study.

The main RIS mechanisms had been understood even before RIS was observed. From the first models, diffusion enhancement and point defect driving forces were accounted for. The kinetic equations are based on general Fick's laws. While in dilute alloys one knows how to deduce such equations from atomic jump frequencies, in concentrated alloys more empirical methods are used. In particular, the definition of the partial diffusion coefficients of the Fick's laws in terms of the phenomenological L-coefficients of TIP has been lost over the years. This can be explained by the lack of diffusion data and diffusion theory to determine the L-coefficients from atomic jump frequencies. For years, the available diffusion data consisted mainly of tracer diffusion coefficients, and the RIS models employed empirical Manning relations, which approximated partial diffusion coefficients based on tracer diffusion coefficients. However, recent improvements of the mean-field diffusion theories, including short-range order effects for both vacancy and interstitial diffusion mechanism, are such that we can expect the development of more rigorous RIS models for concentrated alloys. It now seems possible to overcome the artificial dichotomy between dilute and concentrated RIS models and develop a unified RIS model with, for example, the prediction of the whole kinetic coupling induced by an impurity addition in a concentrated alloy. Meanwhile, first-principles methods relying on the DFT have improved so fast in the last decades that they are able to provide us with activation energies of both vacancy and interstitial jump frequencies as a function of local environment. Therefore, it now seems easier to calculate the L-coefficients and their associated partial diffusion coefficients from first-principles calculations rather than estimating them from diffusion experiments.

An alternative approach to continuous diffusion equations is the development of atomistic-scale simulations, such as mean-field equations or Monte Carlo simulations, which are quite appropriate to study the nanoscale RIS phenomenon. Although the mean-field approach did not reproduce the whole flux coupling due to the neglect of correlation effects, it predicted the main trends of RIS in austenitic steels, with respect to temperature and composition, and was useful to understand the interplay between thermodynamics and kinetics during the formation of an oscillating transitory profile. Monte Carlo simulations are now able to embrace the full complexity of RIS phenomena, including vacancy and split interstitial diffusion mechanisms, the whole flux coupling, the resulting segregation, and eventual nucleation at grain boundaries. But these simulations become heavy time-consuming when correlation effects are important.

Acknowledgments

Part of this work was performed in the framework of the FP7 Perform and GetMat projects. The authors want to thank M. Vankeerberghen for his useful remarks.

References

1. Russell, K. *Prog. Mater. Sci.* **1984**, *28*, 229–434.
2. Holland, J. R.; Mansur, L. K.; Potter, D. I. *Phase Stability During Radiation*; TMS-AIME: Warrendale, PA, 1981.
3. Nolfi, F. V. *Phase Transformations During Irradiation*; Applied Science: London and New York, 1983.
4. Ardell, A. J. In *Materials Issues for Generation IV Systems*; Ghetta, V., *et al.,* Eds.; Springer, 2008; pp 285–310.
5. Was, G. *Fundamentals of Radiation Materials Science*; Springer-Verlag: Berlin, 2007.
6. Allnatt, A. R.; Lidiard, A. B. *Atomic Transport in Solids*; Cambridge University Press: Cambridge, 2003.
7. Meslin, E.; Fu, C.; Barbu, A.; Gao, F.; Willaime, F. *Phys. Rev. B* **2007**, *75*, 094303.
8. Manning, J. R. *Phys. Rev. B* **1971**, *4*, 1111.
9. Barbe, V.; Nastar, M. *Phys. Rev. B* **2007**, *76*, 054206.
10. Barbe, V.; Nastar, M. *Phys. Rev. B* **2007**, *76*, 054205.
11. Wolfer, W. *J. Nucl. Mater.* **1983**, *114*, 292–304.
12. Nastar, M.; Bellon, P.; Martin, G.; Ruste, J. Role of interstitial and interstitial-impurity interaction on irradiation-induced segregation in austenitic steels. In *Proceedings of the 1997 MRS Fall Meeting: Symposium B, Phase Transformations and Systems Driven Far from Equilibrium*, 1998; Vol. 481, pp 383–388.
13. Nastar, M. *Philos. Mag.* **2005**, *85*, 641–647.
14. Grandjean, Y.; Bellon, P.; Martin, G. *Phys. Rev. B* **1994**, *50*, 4228–4231.
15. Soisson, F. *Philos. Mag.* **2005**, *85*, 489.
16. Soisson, F. *J. Nucl. Mater.* **2006**, *349*, 235–250.
17. Rottler, J.; Srolovitz, D. J.; Car, R. *Philos. Mag.* **2007**, *87*, 3945.
18. Anthony, T. R. *Acta. Metall.* **1969**, *17*, 603–609.
19. Anthony, T. R. *J. Appl. Phys.* **1970**, *41*, 3969–3976.
20. Anthony, T. R. *Phys. Rev. B* **1970**, *2*, 264.
21. Anthony, T. R. *Acta Metall.* **1970**, *18*, 307–314.
22. Anthony, T. R.; Hanneman, R. E. *Scr. Metall.* **1968**, *2*, 611–614.
23. Kuczynski, G. C.; Matsumura, G.; Cullity, B. D. *Acta Metall.* **1960**, *8*, 209–215.
24. Aust, K. T.; Hanneman, R. E.; Niessen, P.; Westbrook, J. H. *Acta Metall.* **1968**, *16*, 291–302.
25. Anthony, T. R. In *Radiation-Induced Voids in Metals*; Corbett, J. W., Ianniello, L. C., Eds.; US Atomic Energy Commission: Albany, NY, 1972; pp 630–645.
26. Okamoto, P. R.; Harkness, S. D.; Laidler, J. J. *Trans. Am. Nucl. Soc.* **1973**, *16*, 70–70.
27. Okamoto, P. R.; Wiedersich, H. *J. Nucl. Mater.* **1974**, *53*, 336–345.
28. Barbu, A.; Ardell, A. *Scr. Metall.* **1975**, *9*, 1233–1237.
29. Okamoto, P. R.; Rehn, L. E. *J. Nucl. Mater.* **1979**, *83*, 2–23.
30. Marwick, A. *J. Phys. F Met. Phys.* **1978**, *8*, 1849–1861.
31. Smigelskas, A. D.; Kirkendall, E. O. *Trans. AIME* **1947**, *171*, 130–142.
32. Rehn, L.; Okamoto, P.; Wiedersich, H. *J. Nucl. Mater.* **1979**, *80*, 172–179.
33. Rehn, L. E.; Okamoto, P. R. In *Phase Transformations During Irradiation*; Nolfi, F. V., Ed.; Applied Science: London, 1983; pp 247–290.
34. Bakker, H.; Bonzel, H.; Bruff, C.; *et al. Landolt-Bornstein, Numerical Data and Functional Relationships in Science and Technology*; Springer: Berlin, 1990.
35. Legrand, B.; Tréglia, G.; Ducastelle, F. *Phys. Rev. B* **1990**, *41*, 4422.
36. Busby, J.; Was, G. S.; Bruemmer, S. M.; Edwards, D.; Kenik, E. *Mater. Res. Soc. Symp. Proc.* **1999**, *540*, 451.
37. Norris, D. I. R.; Baker, C.; Taylor, C.; Titchmarsh, J. M. Radiation-induced segregation in 20Cr/25Ni/Nb stainless-steel. In *15th International Symposium on Effects of Radiation on Materials*; 1992; Vol. 1125, pp 603–620.
38. Watanabe, S.; Sakaguchi, N.; Hashimoto, N.; Takahashi, H. *J. Nucl. Mater.* **1995**, *224*, 158–168.
39. Duh, T. S.; Kai, J. J.; Chen, F. R. *J. Nucl. Mater.* **2000**, *283–287*, 198–204.
40. Watanabe, S.; Takamatsu, Y.; Sakaguchi, N.; Takahashi, H. *J. Nucl. Mater.* **2000**, *283–287*, 152–156.
41. Marwick, A.; Piller, R.; Sivell, P. *J. Nucl. Mater.* **1979**, *83*, 35–41.
42. Martin, G.; Bellon, P. *Solid State Phys.* **1997**, *50*, 189–331.
43. Sizmann, R. *J. Nucl. Mater.* **1978**, *69–70*, 386–412.
44. Norgett, M. J.; Robinson, M. T.; Torrens, I. M. *Nucl. Eng. Des.* **1975**, *33*, 50–54.
45. Rehn, L. E.; Okamoto, P. R.; Averback, R. S. *Phys. Rev. B* **1984**, *30*, 3073.
46. Kato, T.; Takahashi, H.; Izumiya, M. *J. Nucl. Mater.* **1992**, *189*, 167–174.
47. Lee, E. H.; Maziasz, P. J.; Rowcliffe, A. F. In *Phase Stability During Irradiation*; Holland, J. R., Mansur, L. K., Potter, D. I., Eds.; TMS/AIME: New York, 1981; pp 191–218.
48. Janghorban, K.; Ardell, A. *J. Nucl. Mater.* **1979**, *85–86*, 719–723.
49. Potter, D.; Ryding, D. *J. Nucl. Mater.* **1977**, *71*, 14–24.
50. Potter, D.; Okamoto, P.; Wiedersich, H.; Wallace, J.; McCormick, A. *Acta Metall.* **1979**, *27*, 1175–1185.
51. Cauvin, R.; Martin, G. *J. Nucl. Mater.* **1979**, *83*, 67–78.
52. Cauvin, R.; Martin, G. *Phys. Rev. B* **1981**, *23*, 3322.
53. Sethi, V. K.; Okamoto, P. R. *J. Met.* **1980**, *32*, 5–6.
54. Little, E. *Mater. Sci. Technol.* **2006**, *22*, 491–518.
55. Lu, Z.; Faulkner, R.; Sakaguchi, N.; Kinoshita, H.; Takahashi, H.; Flewitt, P. *J. Nucl. Mater.* **2006**, *351*, 155–161.
56. Brailsford, A. D.; Bullough, R. *Philos. Trans. R. Soc. Lond. A* **1981**, *302*, 87–137.
57. Nichols, F. *J. Nucl. Mater.* **1978**, *75*, 32–41.
58. Glansdorff, P.; Prigogine, I. *Thermodynamic Theory of Structure, Stability and Fluctuations*; Wiley: New York, 1971.
59. Onsager, L. *Phys. Rev.* **1931**, *37*, 405.
60. Cahn, J. W.; Hilliard, J. E. *J. Chem. Phys.* **1958**, *28*, 258–267.
61. Saunders, N.; Miodownik, A. P. CALPHAD (CALculation of PHase Diagrams), *A Comprehensive Guide Pergamon Materials Series*; Cahn, R. W., Eds.; Elsevier: Oxford, 1998; vol. 1.
62. Bronchart, Q.; Le Bouar, Y.; Finel, A. *Phys. Rev. Lett.* **2008**, *100*, 015702–015704.
63. Hanneman, R.; Anthony, T. *Acta Metall.* **1969**, *17*, 1133–1140.
64. Agarwala, P. *Diffusion Processes in Nuclear Materials*; Elsevier Science: Amsterdam, 1992.
65. Acker, D.; Beyeler, M.; Brebec, G.; Bendazzoli, M.; Gilbert, J. *J. Nucl. Mater.* **1974**, *50*, 281–297.
66. Dalla-Torre, J.; Fu, C.; Willaime, F.; Barbu, A.; Bocquet, J. *J. Nucl. Mater.* **2006**, *352*, 42–49.
67. Henry, J.; Barbu, A.; Hardouin-Duparc, A. Microstructure modeling of a 316L stainless steel irradiated with electrons. In *19th International Symposium on Effects of Radiation on Materials*, 2000; Vol. 1366, pp 816–835.
68. Philibert, J. *Atom Movements: Diffusion and Mass Transport in Solids*; Editions de Physique: Les Ulis, France, 1991.
69. Fu, C. C.; Willaime, F. *Compt. Rendus Phys.* **2008**, *9*, 335–342.

70. Domain, C.; Becquart, C. S. *Phys. Rev. B* **2001**, *65*, 024103.
71. Fu, C. C.; Willaime, F.; Ordejon, P. *Phys. Rev. Lett.* **2004**, *92*, 175503.
72. Bocquet, J. *Defect Diffus. Forum* **2002**, *203–205*, 81–112.
73. Finel, A. In *Phase Transformations and Evolution in Materials*; Turchi, P. E. A., Gonis, A., Eds.; TMS: Warrendale, PA, 2000; p 371.
74. Castin, N.; Malerba, L. *J. Chem. Phys.* **2010**, *132*, 074507.
75. Castin, N.; Malerba, L.; Bonny, G.; Pascuet, M. I.; Hou, M. *Nucl. Instru. Meth. Phys. Res. B* **2009**, *267*, 3002–3008.
76. Martin, G.; Soisson, F. In *Handbook of Materials Modeling*; Yip, S., Ed.; Springer: Netherlands, 2005; pp 2223–2248.
77. Becquart, C. S.; Domain, C. *Phys. Status Solidi B* **2010**, *247*, 9–22.
78. Le Bouar, Y.; Soisson, F. *Phys. Rev. B* **2002**, *65*, 094103.
79. Soisson, F.; Martin, G. *Phys. Rev. B* **2000**, *62*, 203–214.
80. Soisson, F.; Fu, C. *Solid State Phenom.* **2007**, *129*, 31–39.
81. Clouet, E.; Nastar, M. In *Complex Inorganic Solids: Structural, Stability, and Magnetic*; Turchi, P., Gonis, A., Rajan, K., Meike, A., Eds.; Springer-Verlag: New York, 2005; pp 215–239.
82. Allnatt, A. R. *J. Phys. C Solid State Phys.* **1982**, *15*, 5605–5613.
83. Barbe, V.; Nastar, M. *Philos. Mag.* **2007**, *87*, 1649–1669.
84. Nastar, M. *Philos. Mag.* **2005**, *85*, 3767–3794.
85. Allnatt, A.; Barbu, A.; Franklin, A.; Lidiard, A. *Acta Metall.* **1983**, *31*, 1307–1313.
86. Barbu, A. *Acta Metall.* **1980**, *28*, 499–506.
87. Barbu, A.; Lidiard, A. *Philos. Mag. A* **1996**, *74*, 709–722.
88. Doan, N. *J. Phys. Chem. Solids* **1972**, *33*, 2161–2166.
89. Cahn, R.; Haasen, P. *Physical Metallurgy*, 4th ed.; North Holland: Amsterdam, 1996.
90. Bocquet, J. L. *Phys. Rev. B* **1994**, *50*, 16386.
91. Moleko, L. K.; Allnatt, A. R.; Allnatt, E. L. *Philos. Mag. A* **1989**, *59*, 141–160.
92. Barbe, V.; Nastar, M. *Philos. Mag.* **2006**, *86*, 1513–1538.
93. Bakker, H. *Philos. Mag. A* **1979**, *40*, 525–540.
94. Stolwijk, N. *Phys. Status Solidi A* **1981**, *105*, 223–232.
95. Kikuchi, R.; Sato, H. *J. Chem. Phys.* **1970**, *53*, 2702–2713.
96. Kikuchi, R.; Sato, H. *J. Chem. Phys.* **1972**, *57*, 4962–4979.
97. Sato, H.; Kikuchi, R. *Acta Metall.* **1976**, *24*, 797–809.
98. Nastar, M. *Compt. Rendus Phys.* **2008**, *9*, 362–369.
99. Nastar, M.; Barbe, V. *Faraday Discuss.* **2007**, *134*, 331–342.
100. Nastar, M.; Clouet, E. *Phys. Chem. Chem. Phys.* **2004**, *6*, 3611–3619.
101. Barbe, V.; Nastar, M. *Philos. Mag.* **2006**, *86*, 3503–3535.
102. Wiedersich, H.; Okamoto, P.; Lam, N. *J. Nucl. Mater.* **1979**, *83*, 98–108.
103. Howard, R. E.; Lidiard, A. B. *Rep. Prog. Phys.* **1964**, *27*, 161–240.
104. Perks, J. M.; Murphy, S. M. *Materials for Nuclear Reactor Core Applications*; BNES: London, 1987.
105. Johnson, R. A.; Lam, N. Q. *Phys. Rev. B* **1976**, *13*, 4364.
106. Faulkner, R.; Song, S.; Flewitt, P.; Fisher, S. *J. Mater. Sci. Lett.* **1997**, *16*, 1191–1194.
107. Lidiard, A. B. *Philos. Mag. A* **1999**, *79*, 1493.
108. Murphy, S.; Perks, J. *J. Nucl. Mater.* **1990**, *171*, 360–372.
109. Murphy, S. *J. Nucl. Mater.* **1991**, 182, 73–86.
110. Bocquet, J. *Res. Mech.* **1987**, *22*, 1–44.
111. Hashimoto, T.; Isobe, Y.; Shigenaka, N. *J. Nucl. Mater.* **1995**, *225*, 108–116.
112. Shepelyev, O.; Sekimura, N.; Abe, H. *J. Nucl. Mater.* **2004**, *329–333*, 1204–1207.
113. Allen, T. R.; Was, G. S. *Acta Mater.* **1998**, *46*, 3679–3691.
114. Sakaguchi, N.; Watanabe, S.; Takahashi, H. *J. Mater. Sci.* **2005**, *40*, 889–893.
115. Barashev, A. *Philos. Mag. Lett.* **2002**, *82*, 323–332.
116. Sorokin, M.; Ryazanov, A. *J. Nucl. Mater.* **2006**, *357*, 82–87.
117. Barashev, A. V. *Philos. Mag.* **2005**, *85*, 1539–1555.
118. Soisson, F.; Fu, C. *Solid State Phenom.* **2008**, *139*, 107.
119. Barashev, A. V.; Arokiam, A. C. *Philos. Mag. Lett.* **2006**, *86*, 321.
120. Stepanov, I.; Pechenkin, V.; Konobeev, Y. *J. Nucl. Mater.* **2004**, *329*, 1214–1218.
121. Benkaddour, A.; Dimitrov, C.; Dimitrov, O. *J. Nucl. Mater.* **1994**, *217*, 118–126.
122. Mansur, L.; Yoo, M. *J. Nucl. Mater.* **1978**, *74*, 228–241.
123. Hackett, M.; Najafabadi, R.; Was, G. *J. Nucl. Mater.* **2009**, *389*, 279–287.
124. Sakaguchi, N.; Watanabe, S.; Takahashi, H.; Faulkner, R. G. *J. Nucl. Mater.* **2004**, *329–333*, 1166–1169.
125. Soisson, F.; Fu, C. *Phys. Rev. B* **2007**, *76*, 214102–214112.
126. Vincent, E.; Becquart, C.; Domain, C. *J. Nucl. Mater.* **2008**, *382*, 154–159.
127. Vincent, E.; Becquart, C.; Domain, C. *Nucl. Instrum. Methods Phys. Res. B* **2007**, *255*, 78–84.
128. Young, W.; Elcock, E. W. *Proc. R. Soc. Lond.* **1966**, *89*, 735–746.
129. Bortz, A. B.; Kalos, M. H.; Lebowitz, J. L. *J. Comput. Phys.* **1975**, *17*, 10–18.
130. Krasnochtchekov, P.; Averback, R. S.; Bellon, P. *Phys. Rev. B* **2007**, *75*, 144107.
131. Krasnochtchekov, P.; Averback, R.; Bellon, P. *JOM* **2007**, *59*, 46–50.
132. Monasterio, P.; Wirth, B.; Odette, G. *J. Nucl. Mater.* **2007**, *361*, 127–140.
133. Wirth, B.; Odette, G. *Microstr. Processes Irradiat. Mater.* **1999**, *540*, 637–642.